Deletion of a non-canonical promoter regulatory element causes loss of *Scn1a* expression and epileptic phenotypes in mice

Jessica L. Haigh[1,2*], Anna Adhikari[1,3*], Nycole A. Copping[1,3], Tyler Stradleigh[1,2], A. Ayanna Wade[1,2], Rinaldo Catta-Preta[1,2], Linda Su-Feher[1,2], Iva Zdilar[1,2], Sarah Morse[1,2], Timothy A Fenton[1,3], Anh Nguyen[1,2], Diana Quintero[1,2], Michael Sramek[1,2], Jasmine Carter[1,2], Andrea Gompers[1,2], Jason Lambert[1,2], Cesar P. Canales[1,2], Len A. Pennacchio[4,5], Axel Visel[4,5,6], Diane E. Dickel[4,5], Jill L. Silverman[1,3], Alex S. Nord[1,2]

[1]Department of Psychiatry and Behavioral Sciences, University of California, Davis, Davis, CA, USA

[2]Department of Neurobiology, Physiology and Behavior, University of California, Davis, Davis, CA, USA

[3]MIND Institute, University of California, Davis, Davis, CA, USA.

[4]Environmental Genomics and Systems Biology Division, Lawrence Berkeley National Laboratory, Berkeley, CA, USA; U.S. Department of Energy Joint Genome Institute, Walnut Creek, CA, USA; Comparative Biochemistry Program, University of California, Berkeley, Berkeley, CA, USA.

[5]Environmental Genomics and Systems Biology Division, Lawrence Berkeley National Laboratory, Berkeley, CA, USA.

[6]School of Natural Sciences, University of California, Merced, CA, USA

Corresponding author email: asnord@ucdavis.edu

*These authors contributed equally

Abstract

Genes with multiple co-active promoters appear common in brain, yet little is known about functional requirements for these potentially redundant genomic regulatory elements. *SCN1A,* which encodes the $Na_V1.1$ sodium channel alpha subunit, is one such gene with two co-active promoters. Mutations in *SCN1A* are associated with epilepsy, including Dravet Syndrome (DS). The majority of DS patients harbor coding mutations causing *SCN1A* haploinsufficiency, however putative causal non-coding promoter mutations have been identified. To model the functional role of potentially redundant *Scn1a* promoters, we focused on the non-coding *Scn1a* 1b regulatory region, previously described as a non-canonical alternative transcriptional start site. Mice harboring deletion of the extended evolutionarily-conserved 1b non-coding interval exhibited surprisingly severe reduction of *Scn1a* and $Na_V1.1$ expression in brain with accompanying seizures and behavioral deficits. This identified the 1b region as a critical disease-relevant regulatory element and provides evidence that non-canonical and apparently redundant promoters can have essential function.

Introduction

A large proportion of brain-expressed and indeed all mammalian genes are believed to rely on multiple alternative promoters[1–3]. For many genes, the alternative promoters produce distinct 5' untranslated regions that are not translated, leading to identical proteins from distinct transcription start sites (TSSs)[4,5]. Much of the focus on understanding the role of alternative promoters in mammalian transcriptional regulation has been on the potential for discrete function enabling compartmentalized expression in specific cells or tissues[6–9]. However, TSS activity mapping has found many genes where alternative promoters are active in the same tissue[10,11]. More recent evidence from single cell RNA sequencing and chromosome conformation suggests that annotated alternative promoters are frequently co-active in the same cells and physically interact in the nucleus[12–14]. However, in contrast to work on the requirement for alternative promoters with presumed discrete activity, studies investigating the functional requirement for apparently redundant co-active promoters are lacking.

Epilepsy is one of the most common neurological disorders, with both rare highly-penetrant and common variants contributing to genetic etiology. Mutations in *SCN1A,* which encodes the $Na_V1.1$ sodium channel alpha subunit, result in a range of epilepsy phenotypes from generalized febrile seizures to Dravet Syndrome (DS), a severe childhood-onset disorder[15–17]. The majority of DS cases are caused by heterozygous *de novo* mutations in *SCN1A* resulting in truncation of the protein, with haploinsufficiency of $Na_V1.1$ presumed to underlie pathology[18,19]. Mouse models with heterozygous coding mutations in *Scn1a* recapitulate features of DS, including seizures and sudden unexpected death in epilepsy (SUDEP)[20–26]. DS remains pharmacoresistant, with generalized tonic-clonic seizures beginning in the first year of life and comorbidities developing including cognitive impairment, ataxia and SUDEP[27–29]. *SCN1A* transcripts have a variable 5' untranslated region (UTR) containing one of two TSSs, 1a and 1b, that are conserved between human and mouse[30,31]. The proteins produced from 1a and 1b are expected to be identical. 1a (also referred to as h1u) has been defined as the major *SCN1A* promoter, however, comparison across brain tissues in human and mouse suggests that 1a and 1b are co-active, with ~35% of transcripts arising from

1b[30]. The apparent functional redundancy of 1a and 1b promoter activity and of 1a- and 1b-associated SCN1A transcripts raises the question of whether there are distinct roles or requirement of the transcribed 1a and 1b UTR and associated regulatory sequences.

In addition to serving as an example in which to dissect the role of multiple co-active promoters, there is high disease relevance for understanding the functional requirements for *SCN1A* regulatory DNA. *SCN1A* is one of the most common and well-documented genes associated with severe medical consequences of haploinsufficiency. Further, genome-wide association studies (GWAS) have implicated non-coding *SCN1A* DNA variants as contributing to epilepsy risk[32,33], presumably via more subtle perturbation to transcriptional regulation, and non-coding promoter deletions have been found in DS patients[34,35]. A recent study of common variation in the promoter regions of *SCN1A* found that promoter variant haplotypes reduced luciferase in cells and that such non-coding variants in the functional *SCN1A* allele may modify DS severity[36]. Based on these findings, it is plausible that pathogenic variation in regulatory regions modulates *SCN1A* transcription, contributing to epilepsy. Functional studies are needed to determine the consequences of perturbations to *SCN1A* expression caused by mutations in non-coding DNA. Here, we used *Scn1a* as a model for examining transcriptional and phenotypic consequences associated with loss of a potentially redundant co-active promoter. Combining genomics, neuroanatomy, behavior, and EEG, we show that the *Scn1a* 1b non-canonical promoter and flanking conserved non-coding DNA sequence is independently essential for expression and brain function via characterizing the impact of 1b knockout in mice. In addition to mapping an essential regulatory region of a critical disease-relevant gene, our findings provide evidence that non-canonical promoters may play essential roles in general transcriptional activation.

Results

Scn1a 1a and 1b chromosomal regions physically interact and share chromatin signatures indicating pan-neuronal transcriptional activator regulatory activity

To define the regulatory landscape of the *SCN1A* locus, we examined publicly-available chromosome conformation (Hi-C), transcriptomic and epigenomic data obtained from

analysis of human and mouse brain tissues (**Fig. 1a-d**). We generated contact heatmaps from published Hi-C from prefrontal cortex[37] (PFC) at 10-kb resolution (**Fig. 1a**), and for additional tissues at 40-kb resolution[37] (**Fig. S1**). In PFC, *SCN1A* was located at the boundary of two major TADs (Topological Associated Domains), with extensive local interactions within the *SCN1A* locus. Differential analysis of Hi-C from PFC versus lung showed stronger local interactions in PFC, while there were no major differences between the PFC and hippocampus, suggesting brain-specific local *SCN1A* chromosomal interactions (**Fig. 1b** and **Fig. S1**).

Previous work using 5' RACE[30] and luciferase assays defined regulatory sequences at *SCN1A*, including two genomic intervals, non-coding exons 1a and 1b, that are conserved between human and mouse and where the majority of *SCN1A* transcripts originate[30] (**Fig. 1c**). 1a (GenBank: DQ993522) was found to be the majority TSS for *SCN1A* transcripts across human and mouse (54% and 52% RACE transcripts, respectively). 1b (GenBank: DQ993523) was annotated as an alternative TSS, with 25% and 35% of *SCN1A* transcripts originating at this locus in both human and mouse. No strong region-specific differences in 1a versus 1b TSS usage across brain regions were identified in previous work[30,38]. DNA sequence at 1a and 1b is highly evolutionarily-conserved across vertebrates. Notably, conservation at 1b extends nearly 3 kb downstream of the defined UTR transcribed sequence. Interaction models from an independent capture Hi-C dataset[37] also suggested physical interaction between 1a and 1b as well as between 1b and the nearby *TTC21B* promoter (**Fig. 1c**).

We examined chromatin state at the *SCN1A* locus across seven histone post-translational modifications (PTMs) from human mid frontal lobe[39] (**Fig. 1c**). The strongest chromatin signatures for regulatory elements were at the previously-defined 1a and 1b loci, with H3K27ac, H3K4me3 and H3K9ac, weak H3K4me1, and absence of H3K27me3, H3k9me3, H3K36me3 in these regions. In ATAC-seq and H3K27ac across the majority of non-CNS tissues profiled in the ENCODE or Roadmap projects, 1a and 1b show reduced or absent signal, further indicating primary importance in the nervous system (data not shown). In addition to 1a and 1b, there were several other non-coding regions showing weaker, but still significant enrichment for H3K27ac in brain,

representing potential additional *SCN1A* regulatory elements. ATAC-seq from neuronal and non-neuronal cells from dorsolateral PFC (DLPFC)[40] showed that neuronal cells have increased chromatin accessibility across *SCN1A* generally (**Fig. 1c**), with specific enrichment at 1a, 1b, and a third region also within the first intron of *SCN1A*. Comparing human neuronal data with mouse ATAC-seq and histone PTM data[41], accessibility and chromatin states appeared largely conserved (**Fig. 1c** and **1d**). Finally, ATAC-seq data[41] from sorted neuronal subtypes in mouse, including excitatory neurons and parvalbumin (PV) and vasointestinal peptide (VIP) interneurons, indicated no difference in open chromatin signatures for the *Scn1a* locus and 1a and 1b across neuron types (**Fig. 1d**).

The evolutionarily-conserved Scn1a 1b non-coding region acts as a Scn1a transcriptional activator and is essential for survival

Taken together, the comparative and functional genomics data indicates evolutionarily conserved brain-specific pan-neuronal regulatory and TSS activity of 1a and 1b and chromosomal physical interaction between the two promoters. The 1b region has been annotated as an alternative TSS, yet the extended region surrounding the annotated transcribed UTR also shows the strongest enrichment across non-coding DNA at the *SCN1A* locus for evolutionary conservation and for chromatin signatures indicating enhancer and promoter activity (i.e. H3K27ac and H3K4me3). We sought to validate the specific role of 1b DNA in activation of *SCN1A* expression. We used luciferase assay to functionally test the core human 1b (h1b) region in cell lines. A 941 bp region containing 1b and conserved flanking sequence induced expression in HEK293 and SK-N-SH cells when cloned into a vector with a minimal promoter (**Fig. 1e**). To further demonstrate the regulatory role of 1b in *SCN1A* expression, we showed that a pool of 6 sgRNAs targeted to human 1b sequence and delivered along with dCas9-p300, a histone acetyltransferase, was sufficient to induce *SCN1A* expression 2.5-fold in HEK293 cells compared to non-transfected control (**Fig. 1f**).

The strength of evolutionary conservation and transcriptional activation-associated epigenomic signatures at the extended 1b interval is paradoxical considering its

presumed role as a secondary TSS. Thus, we sought to test whether the extended 1b regulatory region is essential for *Scn1a* expression, and whether loss of this element is sufficient produce epilepsy and DS-relevant phenotypes in mouse. We used CRISPR/Cas9 targeting of C57BL/6N oocytes to generate mice harboring a 3063 bp deletion of the interval flanking the 1b regulatory element of *Scn1a*, removing the entire mammalian conserved region (**Fig. 2a**). We identified an F0 mutation carrier that transmitted the deletion to F1 offspring and confirmed the deletion interval via Sanger sequencing (**Fig. 2b**). We expanded this *Scn1a* 1b deletion line and eliminated potential off-target Cas9-induced mutations via breeding to wildtype C57BL/6N (WT) mice.

Previous work found that mice harboring homozygous coding mutations to *Scn1a* die in the third postnatal week and mice with heterozygous coding mutation exhibit reduced survival[20,26]. In comparison, 46 female WT by male heterozygous 1b harem trios pairings yielded 41 litters (**Fig. 2c**) and survival rates of WT and heterozygous 1b deletion pups were indistinguishable (**Fig. 2d**, $p>0.9999$, Chi squared with Fisher's exact test), indicating reduced severity of 1b deletion in comparison to coding loss-of-function mutation. However, female heterozygous 1b by male heterozygous 1b harem trios required nearly double the number of pairings at 74 and produced only 18 litters (**Fig. 2c**). Further, survival rates for WT and heterozygous 1b pups from these litters were indistinguishable ($p>0.9999$), but 42% of homozygous 1b deletion mice died by weaning (**Fig. 2d**, $p=0.0005$). We additionally tested heterozygous 1b deletion mice for measures of general health, finding no consistent deficits in growth, reflexes, and limb strength (**Table S1**). Thus, heterozygous S*cn1a* 1b deletion mice survive, but female deletion carriers fail to produce litters, indicating behavioral or physiological deficits associated with 1b deletion in females. Due to breeding and survival issues we include limited numbers of homozygous *Scn1a* 1b deletion mice in further analyses.

Loss of extended 1b interval causes loss of $Na_V1.1$ across postnatal brain regions

We first sought to characterize changes in distribution and amount of $Na_V1.1$ protein caused by loss of 1b in postnatal mouse brain. Reduction in protein expression across the mouse brain was confirmed by Western blot analysis of hippocampus from 3-month-

old mice, showing that both heterozygous and homozygous 1b deletion resulted in decreased $Na_V1.1$ protein expression compared to WT (**Fig. 2e**). $Na_V1.1$ expression was reduced by 36% in heterozygous mice and 62% in homozygous deletion mice in the hippocampus. A similar change in protein expression was measured in the cerebellum with a 41% reduction in heterozygous mice and 63% in deletion mice (**Fig. 2e**). Raw western blots can be seen in supplementary (**Fig. S2**).

$Na_V1.1$ immunohistochemistry (IHC) in WT mice showed expression across cerebellum, hippocampus and cortex (**Fig. 2fi-iii**), consistent with previous studies of RNA and protein expression. We compared expression of $Na_V1.1$ along with the interneuron marker parvalbumin across 1b homozygous deletion, heterozygous deletion, and WT mice (**Fig. 2g**). Notably, deletion of 1b appeared to generally ablate $Na_V1.1$ expression, rather than specifically impact certain brain regions, consistent with 5' RACE TSS activity[30]. There was no obvious qualitative change in $Na_V1.1$ IHC between WT and heterozygous 1b deletion mice, while homozygous deletion mice had obvious reduction of expression in the brainstem, cerebellum and hippocampus.

Differential gene expression in in Scn1a 1b deletion mouse hippocampus

First, we tested for expected reduced *Scn1a* RNA expression via quantitative reverse-transcription PCR (qRT-PCR) performed on cortex, hippocampus and cerebellum of 3-month-old *Scn1a* 1b deletion carriers and WT littermates (**Fig. 3a**). In agreement with GTEx[38] and previous studies[30], we observed the highest level of WT *Scn1a* expression in the cortex with expression in cerebellum and hippocampus 34% and 60% lower, respectively. When comparing 1b deletion to WT mice, there was a trend for reduction in *Scn1a* expression in heterozygous 1b deletion mice, and homozygous 1b deletion carriers had a significant reduction to approximately 40% WT in all regions. These results are consistent with Western blot results indicating that deletion of the extended 1b interval had a larger than expected impact on *Scn1a* and $Na_V1.1$ expression considering the proportion of transcripts expected to originate at this element.

We next used RNA sequencing (RNA-seq) on P7 forebrain from WT (n=2), heterozygous (n=4) and homozygous (n=2) 1b deletion mice and P32 micro-dissected

hippocampus tissue from WT (n=2), heterozygous (n=2) and homozygous (n=2) 1b deletion mice. For both P7 and P32, *Scn1a* expression showed significant dosage dependent decrease using an additive model (**Table S4**, **S5**). Considering the individual genotypes, *Scn1a* expression was significantly reduced compared to WT in homozygous 1b deletion knockout mice at P7 and P32, and intermediate, but not significantly different, *Scn1a* expression was observed in heterozygous 1b deletion carriers (**Fig. 3b**), consistent with qRT-PCR data. To compare transcripts arising from either 1a or 1b at P32, when *Scn1a* expression in WT brain is high, we measured the number of splice junction reads that linked the 1a and 1b non-coding exons with the first *Scn1a* coding exon and the number that mapped unambiguously to 1a or 1b (**Fig. 3c**). As expected, splice junction and overlapping reads associated with mouse 1b (m1b) were reduced in heterozygous 1b deletion mice and abolished in homozygous 1b deletion mice. While 1a (m1a) splice junction and overlapping reads were not significantly reduced in heterozygous or homozygous 1b deletion carriers, relatively few reads were identified. The change in total *Scn1a* reads from RNA-seq (**Fig. 3b-c**) was consistent with qRT-PCR and $Na_V1.1$ western blot data, indicating much higher than anticipated decrease in RNA and protein levels considering the proportion of *Scn1a* transcripts originating at 1b. These findings are inconsistent with a model where 1b deletion specifically and solely impacts 1b transcript levels without affecting levels of *Scn1a* transcripts originating at 1a or other minor TSSs.

We tested for differential expression across 9260 and 8460 genes that were robustly expressed in the P7 and P32 RNA-seq datasets, respectively. As heterozygous 1b deletion carriers were more variable in *Scn1a* expression and transcriptomic signature (**Fig. 3b, S3a**), we focused analysis on comparison of homozygous 1b deletion carriers with WT littermates. At P7, *Scn1a* was the only differentially expressed (DE) gene specific to homozygous 1b deletion mice using a threshold of FDR < 0.05 (**Table S6**). The minimal effect of 1b deletion on genes other than *Scn1a* at P7 is consistent with the low expression and non-essential role of *Scn1a* in early postnatal development[42]. In contrast, at P32 a total of 723 genes (337 downregulated, 386 upregulated) were DE at FDR < 0.05. Volcano plots for DE genes in homozygous null versus WT mice shown in **Fig. 3d**, with heterozygous versus WT mice in **Fig. S3b**. Gene set enrichment analysis

of Gene Ontology (GO) terms for homozygous 1b deletion mice (**Fig. 3e**) found enrichment for genes associated with neuron development and differentiation in upregulated genes, in contrast genes for synaptic signaling and mature neuronal function were enriched among downregulated genes. The P32 DE signatures of downregulated synaptic expression and upregulated expression of earlier neuronal differentiation and maturation genes are consistent with previous data on *Scn1a* coding mutants[43]. These DE results could be driven by either developmental changes or reflect the transcriptional responses to seizures in 1b deletion mice[43].

Homozygous but not heterozygous 1b deletion causes cognitive deficits in novel objection recognition (NOR) and spontaneous alternation in the Y-maze

To investigate the impact of 1b deletion on behavior, we performed a tailored battery focused on learning and memory and motor abilities. Heterozygous 1b deletion mice were additionally tested in a comprehensive behavioral battery of standard assays of overall physical health across development, sensorimotor reflexes, motor coordination, anxiety-like, and social behavior. A summary of the results from these experiments is reported in **Table S2**. Both heterozygous and surviving homozygous 1b deletion mice were comparable to WT littermates in developmental milestones.

Cognitive deficits were observed in homozygous 1b deletion but not heterozygous mutant mice by two corroborating assays of learning and memory, NOR and Y-maze. Following established NOR methods[44,45] manual scoring by a highly-trained observer blinded to genotype indicated WT and heterozygous 1b deletion mice spent more time investigating the novel object versus the familiar object, as expected. In contrast, homozygous 1b deletion mice did not exhibit typical novel object preference (**Fig. 4a**: Two-way repeated measures for genotype $F(2, 73) = 3.487$, $p < 0.04$ and object $F(1, 73) = 14.77$, $p < 0.0003$). Comparisons between the novel object versus the familiar object significantly differed in the WT ($p = 0.002$) and heterozygous 1b deletion mice ($p = 0.018$), illustrating recall of the familiar object and learning. Yet the null mutant mice did not exhibit this typical recall ($p = 0.8698$). Sexes were combined since there was no sex difference observed on time spent sniffing objects (**Table S3**). Control data

illustrating no preference for the left or right objects and sufficient time spent investigating the objects is shown in **Fig. 4b**. Homozygous 1b deletion mice were also impaired on the Y-maze, making less alternation triads compare to WT and heterozygous 1b deletion carriers (**Fig. 4c**: $F(2, 62) = 5.693$, $p < 0.005$). Sidak's multiple comparisons indicated the homozygous 1b mutants differed from the WT ($p = 0.0192$) and heterozygous 1b deletion ($p = 0.0047$) mice.

Most parameters of gross motor skills and motor coordination were similar across genotypes (**Table S2**). In the open field novel arena assay of locomotion, homozygous 1b deletion mutants were hyperactive during 10 minutes of the 30-min session. The time course for horizontal, total and vertical activity was typical across time, representing normal habituation to the novelty of the open field in all genotypes. Horizontal and vertical activity did not differ between genotypes (**Fig. 4d-e**; $F(2, 80) = 0.1401$, $p > 0.05$). However, homozygous 1b deletion mice were hyperactive in total activity (**Fig. 4f**; $F(2, 80) = 5.117$, $p < 0.008$, Two-Way repeated measures ANOVA). Sidak's multiple comparisons indicated comparisons between the homozygous 1b deletion versus the WT mice differed at time of minutes 11-15 ($p = 0.0014$) and differed between the homozygous and heterozygous 1b deletion mice at time of minutes 11-15 ($p < 0.0001$) and 16-20 ($p = 0.0270$). In addition to indicating that homozygous 1b deletion causes hyperactivity, which is linked to DS[46,47], these results indicate that there were no gross motor abnormalities, inability to rear, or hindlimb weakness that would prevent exploration of objects in NOR and confound that assy.

Heterozygous 1b deletion mice did not exhibit significant consistent phenotypes in learning and memory assays or a comprehensive battery of assays standard for examining mouse models of neurodevelopmental disorders (**Table S2**). Heterozygous 1b mice spent less time in the dark chamber in the light-dark assay ($T(69) = 2.121$, $p = 0.0375$, unpaired two-tailed t-test) and had decreased ultrasonic vocalizations ($T(25) = 2.143$, $p = 0.0420$, unpaired two-tailed t-test), but in the absence of corroborating assays for anxiety and socialization these results are only suggestive.

Adult mice harboring heterozygous 1b deletion are susceptible to seizures and exhibit abnormal EEG activity

We next tested for epilepsy-relevant phenotypes in heterozygous 1b deletion mice using a standard pentylenetetrazole (PTZ) chemoconvulsant seizure induction analysis and using EEG[48]. First, we performed a dose response analysis on mice of the C57BL/6N background strain to identify a dose that allowed for observations of all stages of behavioral seizure in addition to EEG seizures (data not shown). To test for induced seizure susceptibility, heterozygous mice were administered a high-dose (80 mg/kg, i.p.) of PTZ. After administration, latencies to first jerk, loss of righting, generalized clonic-tonic seizure, and full tonic extension were measured. For all measures, reduction in latency, or shorter time to respond, indicated seizure susceptibility associated with heterozygous 1b deletion. PTZ-treated heterozygous 1b deletion mice exhibited seizure susceptibility across all measures (**Fig. 5a-d**: first jerk $t(1, 30) = 2.171$, $p = 0.038$; loss of righting $t(1, 30) = 2.160$, $p = 0.039$; generalized clonic-tonic seizure $t(1, 30) = 2.128$, $p = 0.042$; full tonic extension $t(1, 30) = 2.207$, $p = 0.035$).

To corroborate behavioral seizure susceptibility observed after convulsant induction, intracranial EEG was implemented in a second group of animals to look at the underlying neurophysiology. Spiking activity measured by bouts of spike trains was significantly higher in heterozygous 1b deletion carriers when compared to WT littermate controls (**Fig. 5g**: $t(1, 8) = 3.812$, $p = 0.005$), indicating heightened excitability. Heterozygous 1b deletion carriers also had higher power detected across all frequency bins when compared to controls (**Fig. 5h**: $F(1, 8) = 423.9$, $p < 0.0001$, multiple comparisons all had $p < 0.0001$). PTZ administration in the EEG-analyzed mice reproduced the faster latency to seizure onset and trends towards faster latency to death (**Fig. i-j**: $t(1, 8) = 3.920$, $p = 0.004$, $t(1, 8) = 2.103$, $p = 0.068$). The observed behavioral seizures and epileptiform signatures in EEG have realistic translational relevance[49–51], and the link between 1b deletion and reduced *Scn1a* produced epileptiform phenotypes in the mouse brain validates disease relevance of this model.

Discussion

The majority of focus and functional studies of alternative promoters has been on genes where the multiple alternative TSSs are predicted to have discrete cell-type or tissue-specific activity[6–9]. However, recent studies of TSS usage and promoter interactions suggest a model where alternative promoters interact physically and are co-active in the same cells[12–14]. In these situations, it is largely unknown what the requirement for individual TSS and associated regulatory DNA may be. Here we focus on one specific putative non-canonical disease-relevant alternative promoter, a 3 kb evolutionarily-conserved DNA region including the previously described *Scn1a* 1b TSS. We show that deletion of this interval from the mouse genome causes significant decrease in *Scn1a* expression, $Na_V1.1$ protein, and results in susceptibility to seizures and an epilepsy-relevant neurophysiology phenotype. These results define an essential disease-relevant regulatory region and show that loss of regulatory DNA associated with a non-canonical TSS has an interactive impact on total expression across all start sites.

There are multiple possible explanations for the observed strong impact of loss of the 1b interval on *Scn1a* expression. First, 1a and 1b may indeed be discretely regulated, but previous measures of 1b-originating transcripts must have significantly underestimated the actual proportion of 1b expression. In this case, our findings would simply reflect that 1b is actually the dominant *Scn1a* promoter. While we cannot disprove this, there is no evidence that earlier studies were incorrect and our estimates of 1a and 1b RNA-seq read frequency in 1b deletion mice do not support a model where 1b is dominant. Alternatively, the loss of the 1b genomic interval could result in decreased TSS activity at 1a as well via an interactive effect where 1b-associated regulatory DNA activity is required for 1a transcription. This model is plausible based on evidence for physical interaction of 1a and 1b, the correlation between 1b and 1a chromatin state across neuronal cell types, and the severe reduction in overall *Scn1a* transcript and $Na_V1.1$ protein in 1b deletion mice. Considering the frequency of promoter-promoter interaction and reported common co-expression of alterative TSSs in single neurons, many brain genes could share similar regulatory structure, where regulatory DNA at putative alternative promoters contributes to transcriptional activation

across interacting TSSs. While further experiments are needed to resolve the function of the 1a and 1b intervals and similar studies of other genes are needed to show that this phenomenon is widespread, our findings represent initial insights into the potential essential regulatory roles of non-canonical promoter DNA.

Annotation of the genome has led to major gains in understanding transcriptional wiring, yet it has been surprisingly difficult to predict the sufficiency and necessity of specific regulatory elements, even those expected to be critical based on comparative and functional genomics[3,10,52]. Knockout mouse models have been a gold standard for testing the phenotypic consequences of mutations, and recent efforts deleting non-coding DNA have provided critical insights into the role of regulatory DNA[52–55]. Here, we used CRISPR/Cas9-mediated deletion to assess the role of the evolutionarily-conserved 1b interval on higher order neurological phenotypes. Homozygous 1b deletion caused behavioral deficits and had a strong impact on survival, demonstrating the essential nature of the deleted interval. Our transcriptomics data suggests that homozygous deletion impacts expression of genes relevant to epilepsy, with downregulation on mature synaptic and signaling genes and upregulation of neural maturation and developmental genes. These findings indicate that the extended 1b DNA sequence plays a critical role in *Scn1a* expression. Further studies are needed to define the minimal and core nucleotides within the 1b interval and to define proteins that bind and participate in regulation. In addition, similar functional studies of other *Scn1a* regulatory DNA elements, and specifically of the 1a region, are necessary to determine which regulatory DNA regions are necessary and sufficient for expression in the brain.

In the disease-relevant heterozygous 1b deletion state, we identified susceptibility to induced seizures and epileptiform EEG activity. Thus, our studies show that heterozygous 1b deletion produces epilepsy-relevant phenotypes in mice. Heterozygous loss of the 1b interval appears to have a less severe phenotypic impact compared to heterozygous truncating *Scn1a* mutations. Such truncating mutations reduce survival and cause behavioral and cognitive deficits relevant to DS in mice[20,26] and are more similar to the homozygous 1b deletion phenotype identified here. It is possible that phenotypes are milder in heterozygous 1b deletion mice in this study

compared to previously analyzed DS mouse models due in part to differences in genetic background or environment. Regardless of the specific relevance to DS phenotypes, our results prove that perturbation to 1b function produce cognitive impairments and robust epilepsy-relevant phenotypes, justifying increased focus on non-coding regulatory DNA in genetic screening of DS and epilepsy patients.

While we did not identify corroborated behavioral phenotypes in heterozygous 1b deletion mice, female 1b deletion carriers failed to efficiently reproduce and heterozygous 1b deletion mice exhibited abnormal EEG spectral bandwidths. Thus, it is possible that more subtle neurodevelopmental disorders (NDDs) and DS behavioral and cognitive deficits are caused by heterozygous 1b deletion. Furthermore, the EEG spectral phenotypes in heterozygous 1b deletion mice overlap with other NDD and epilepsy models. Elevated delta spectral power is a biomarker of Angelman Syndrome (AS)[56] and elevated beta spectral power is posited to be a biomarker of Dup15q syndrome[57,58]. These disorders are of interest as there are co-occurring features with DS and epilepsy. AS and Dup15q both have high rates of seizures, cognitive disruption and comorbid diagnosis with autism. Neural signatures in EEG by power bands can be similarly measured in both rodents and humans, and thus our findings have translational relevance[49–51]. Analysis of spike-firing and oscillatory activity during rewarded trials in touchscreen assays have recently been described in detail[59]. Given the behavioral deficits in cognitive function and firing activity identified here, future studies investigating behavioral outcomes and neurophysiological signals are warranted and will shed light on relationship between 1b deletion, EEG spectral phenotypes and behavior.

SCN1A-associated epilepsies, including DS, remain difficult to treat as conventional sodium channel blockers are usually ineffective and may even exacerbate the disease[29,60]. Precision therapies that rescue $Na_V1.1$ haploinsufficiency in relevant cell types would be preferred to ameliorate symptoms and reduce side effects compared to more globally acting therapies. Using CRISPR/dCas9 induction, we increased *SCN1A* expression in HEK293 cells by targeting the 1b region with the histone acetyltransferase p300. Application of a similar synthetic transcriptional activation therapeutic strategy has

shown exciting promise in vivo in mice, where a dCas9-based activator combined with locus-specific guide RNA delivered to hypothalamus was capable of rescuing obesity phenotypes in mice with *Sim1* and *Mc4r* heterozygous mutations, as examples of haploinsufficiency mouse models[61]. It is plausible that *Scn1a* may be amenable to similar strategy via targeting regulatory regions such as 1b. Studies characterizing the regulatory DNA at disease-relevant loci, as we have done here with the *Scn1a* 1b region, will be required to properly design therapies using targeted genomic expression rescue. The work here on the 1b regulatory region represents a first step toward functional dissection of the regulatory wiring of a major epilepsy risk gene. Our findings show that *Scn1a* 1b regulatory deletion mice represent an epilepsy-relevant model that will be valuable for understanding the relationship between *Scn1a* dosage and neurological phenotypes in a genetic preclinical model.

Acknowledgments

Sequencing was performed at the UC Berkeley and UC Davis DNA cores. This work was supported by funds from the Dravet Syndrome Foundation, Simons Foundation Autism Research Initiative and by NIGMS R35 GM119831. L.S.-F. was supported by the UC Davis Floyd and Mary Schwall Fellowship in Medical Research and by grant number T32-GM008799 from NIGMS-NIH. A.A.W. was supported by Training Grant number T32-GM007377 from NIH-NIGMS and F31 MH119789-01. R.C.-P. was supported by a Science Without Borders Fellowship from CNPq (Brazil). A.V., L.A.P. and D.E.D. were supported by National Institutes of Health grants R24HL123879, U01DE024427, R01HG003988, U54HG006997 and UM1HL098166. Research conducted at the E.O. Lawrence Berkeley National Laboratory was performed under Department of Energy Contract DE-AC02-05CH11231, University of California. We also thank Heather Boyle at the MIND Institute for her diligence and assistance with the mouse colonies. This work was supported by generous funding from the NIH R01NS097808 (JLS, NAC, AA) and the MIND Institute's Intellectual and Developmental Disabilities Resource Center (HD079125, PI Abbeduto).

Author contributions

JLH and AA are listed as joint first authors, as each led major components of the study. JLH, AA, NAC, TS, AAW, RCP, LSF, JC, JLS and ASN designed the experiments and analyses. JLH, AA, NAC, TS, IZ, SM, TAF, AN, DQ, MS, JC, AG, JL, CPC, LAP, AV and DED performed experiments. AA, NAC and TAF carried out mouse behavior. LSF, AAW, ASN performed and interpreted transcriptomic analysis. JLH, IZ, SM, AN, DQ, MS, JC ran cell culture experiments. JLH, AA, NAC, JLS and ASN drafted the manuscript. All authors contributed to the revisions

Materials and Methods

Generation of 1b mutant mice

We used Cas9-medaited mutagenesis of C56BL/6N oocytes to generate a mouse line harboring deletion of a conserved portion on the noncoding region of Scn1a containing the previously described 1b[30] regulatory region. Guide RNA was designed and synthesized according to described methods[62], pooled with Cas9 mRNA and injected into mouse oocytes. We identified the unique guides GGAGATCTGGGTAGTCCTCG and GCTTTTCATACTATAGTGAG. Initial Cas9 targeting was performed at Lawrence Berkeley National Laboratory. F0s (induced on C57BL/6N background) carrying mutations were genotyped and bred to expand lines that harbored a mutation. We identified F0 pups carrying a 3063 bp deletion (mm10 - chr2:66407567-66410630) in 1b.

The colony was rederived and maintained by crossing male 1b deletion carriers with C57BL/6N wild-type females (Charles River). Extensive crossing of heterozygous mutation carriers to wild-type animals vastly reduces the likelihood that any potential off-target mutations caused by Cas9 targeting would persist in our 1b deletion line. Genotypes were identified via PCR and sequence-verified for all animals included in analyses, with the primers in Table 1. All mouse studies were approved by the Institutional Animal Care and Use Committees at the University of California Davis and the Lawrence Berkeley National Laboratory. Subject mice were housed in a temperature-controlled vivarium maintained on a 12-h light–dark cycle. Efforts were made to minimize pain and distress and the number of animals used.

Primer name	**Sequence (5'-3')**
L_outer_Scn1a	AGATCAGGCCTTCTTGCTGA
R_outer_Scn1a	GGGCTCCTCATTGTTTTGGG
R_interal_Scn1a	CACACACAGGCACATGATGA

Table 1: Scn1a 1b deletion genotyping primers

RNA collection

Cortex, hippocampus and cerebellum were regionally dissected from one hemisphere of P7, P32 and 3-month-old homozygous deletion, heterozygous and wildtype mice. Both male and female mice were used, though there were not equal sex representation across genotypes. Total RNA was isolated using RNAqueous kit (Ambion) and assayed using an Agilent BioAnalyzer instrument.

qRT-PCR

Differential expression of Scn1a was verified by qRT-PCR at 3 months old. Briefly, 500 ng RNA was used for reverse transcription using SuperScript VILO cDNA synthesis kit (Invitrogen). Primers are reported in Table 2 and qPCR was performed with SYBR green PCR master mix (Applied Biosystems). Samples were excluded if technical replicates failed. Cycle counts were normalized to Gapdh. Statistical analysis was performed using unpaired Student's t-tests on normalized relative gene expression between genotypes using ΔΔCT.

Target	**Sequence (5'-3')**
Human Gapdh	F-CAATGACCCCTTCATTGACC
	R-TTGATTTTGGAGGGATCTCG
Mouse Gapdh	F-TCACCACCATGGAGAAGGC
	R-GCTAAGCAGTTGGTGGTGCA
Scn1a (mouse and human)	F-CTCGTTCCTGATCGTGTTCC
	R-ATCCTGTCCACAGCAATCTG

Table 2: qPCR primers.

RNAseq

RNA from P7 forebrain and P32 hippocampus was collected as described above. Samples included males and females of each genotype. Total RNA was isolated using Ambion RNAqueous and assayed using an Agilent BioAnalyzer instrument. Stranded mRNA sequencing libraries were prepared using TruSeq Stranded mRNA kit. All eight samples were pooled and sequenced in one lane on the Illumina HiSeq platform using a single-end 100-bp strategy. Each library was quantified and pooled before sequencing at the UC Davis DNA Technologies Core.

The transcriptomic analysis was performed as before[63]. Reads from RNA-seq were aligned to the mouse genome (mm9) using STAR (version 2.7.2)[64]. Aligned reads mapping to genes were counted at the gene level using subreads featureCounts[65]. The mm9 knownGene annotation track and aligned reads were used to generate quality control information using the full RSeQC tool suite[66]. Unaligned reads were quality checked using FastQC.

Differential expression analysis

Raw count data for all samples were used for differential expression analysis using edgeR[67]. Genes with at least 20 reads per million in at least one sample were included for analysis, resulting in a final set of 9260 and 8460 genes for differential testing in P32 and P7 mice, respectively. Multidimensional scaling analysis indicated that *Scn1a* expression was the strongest driver of variance across samples. Tagwise dispersion estimates were generated and differential expression analysis was performed using a generalized linear model with genotype as the variable for testing. Efffect of genotype was modelled both additively as the effect per deleted 1b allele, as well as individual comparison of heterozygous and homozygous 1b deletion mice with the WT controls. Sex was used as a factor-based co-variate where equal representation across genotypes was present. Where there was sex bias (P7 samples), sex-linked genes were omitted from analysis. Normalized expression levels were generated using the edgeR rpkm function. Normalized log2(RPKM) values were used for plotting of expression data for Scn1a. Pseudo-count values were used for plotting summary heatmaps. Aligned reads contained in BAM files from each sample were counted to calculate the overlap of sequencing reads with each locus. The coordinates for each locus were m1a: chr2:66,278,753-66,278,887, the m1b deletion region: chr2:66245632-66248697, and m1c: chr2:66,249,400-66,249,514. Mouse gene ontology (GO) data was downloaded from Bioconductor (org.Mm.eg.db). We used the goseq package to test for enrichment of GO terms indicating parent:child relationships. For GO analysis, we examined down- and up-regulated genes separately for genes meeting an FDR < 0.1. For the enrichment analysis, the test set of differentially expressed genes was

compared against the background set of genes expressed in our study based on minimum read-count cutoffs described above.

Immunohistochemistry

All histological experiments were performed at least in triplicate and experimenters were blinded to genotype. Following anesthesia, P28 male and female mice were transcardially perfused with 4% paraformaldehyde (PFA) in HEPES, followed by overnight fixation in the same solution. After fixation, brains were removed from the skull, embedded in 2% LTE agarose/ Tris-buffered saline (TBS) and cut coronally in 50 µm sections on a vibratome (VT 1000S, Leica). Sections were mounted onto glass slides (SuperFrost Plus, Thermo-Fisher) and underwent antigen retrieval in a solution of 0.1 M sodium citrate (pH 6), 200 mM sucrose and 1% (v/v) hydrogen peroxide at 60ºC for one hour. Subsequently, sections were permeabilized and blocked in TBS with 0.1% Triton X-100 and 5% normal donkey serum for 24 hours at room temperature. Immunolabelling was carried out using primary antibodies directed against $Na_V1.1$ (K74/71, mouse, IgG1, 1:100, NeuroMab) and parvalbumin (L114/3, 75-455, mouse, IgG2a, 1:100, NeuroMab). Subclass specific secondary antibodies (488 and RRX) were used at 1:200 (Jackson ImmunoResearch Laboratories Inc.). All imaging was carried out on a Nikon A1 laser scanning confocal microscope.

Western blot

Flash frozen samples were prepared for Western blot by sonication in 2x Laemmli buffer. After sonication, samples were spun down and the supernatant was used for a BCA Bradford assay using the Spectramax 190 plate reader to assess protein concentration using a standard curve. We ran 20 µg of protein on 8% and 12% gels using the Mini-PROTEAN Tetra Cell western blotting system (Bio-Rad). Anti-$Na_V1.1$ (ASC-001, rabbit, 1:1000, Alomone) and anti-Gapdh (chicken, 1:10,000) primary antibodies were incubated overnight in Odyssey blocking buffer (LI-COR), visualized using a LI-COR Odyssey CLx system and quantified in FIJI (National Institutes of Health). Protein levels assayed via western blot were compared by unpaired Student’s t-test.

Mouse colony at UC Davis Medical Center

Heterozygous (+/-) breeders were transferred from the UC Davis Center of Neuroscience to the UC Davis Medical Center. Offspring were maintained on the C57BL/6N background from The Jackson Laboratory (Bar Harbor, ME). Colonies were maintained with two breeding paradigms: wildtype (+/+) by heterozygous (+/-) and heterozygous (+/-) by heterozygous (+/-) crosses, giving rise to wildtype (+/+), heterozygous (+/-), and knockout mice (-/-). Breeding success and efficiency is reported in Results. Approximately, 2-weeks after pairing, females were individually housed and inspected daily for pregnancy and delivery. To identify mice, pups were labelled by paw tattoo on postnatal day (PND) 2-3 using non-toxic animal tattoo ink (Ketchum Manufacturing Inc., Brockville, ON, Canada). At PND 4-7, tails of pups were clipped (1-2 mm) for genotyping, following the UC Davis IACUC policy regarding tissue collection. Genotyping was performed in our Sacramento laboratory with REDExtract-N-Amp (Sigma Aldrich, St. Louis, MO, USA) using primers AGA TCA GGC CTT CTT GCT GA, GGG CTC CTC ATT GTT TTG GG, and GTG TTC ACG GTG CTT TTC AT. After weaning on PND 21, mice were socially housed in groups of 2-4 by sex. All mice were housed in Techniplast cages (Techniplast, West Chester, PA). Cages were housed in ventilated racks in a temperature (68-72°F) and humidity (~25%) controlled vivarium on a 12:12 light/dark cycle with lights on at 07:00, off at 19:00-h. Standard rodent chow and tap water were available ad libitum. In addition to standard bedding, a Nestlet square, shredded brown paper, and a cardboard tube (Jonesville Corporation, Jonesville, MI, USA) were provided in each cage. All subjects were tested between 2-5 months of age and all experimental procedures were performed in accordance with the National Institutes of Health Guide for Care and Use of Laboratory Animals and were approved by the Institutional Animal Care and Use Committees (IACUC) of the University of California, Davis.

Design

Both male and female subjects were used in this study. Subjects began the behavioral battery at 6-weeks of age. All behavioral tests were performed between 09:00 and

17:00-h during the light phase of the 12:12 light/dark cycle. Mice were brought to an empty holding room adjacent to the testing area at least 1-h prior to the start of behavioral testing. Mice were tested in the follow order: open field, spontaneous alternation, and novel object recognition. After completing the behavioral battery, a small subset of mice was used for EEG acquisition and the remaining animals were administered a lethal-dose of pentylenetetrazole to evaluate seizure susceptibility.

Order of testing: elevated plus maze, light dark, open field, spontaneous alternation, novel object recognition, self-grooming, beam walking, rotarod, social approach, male-female social interaction, acoustic startle, pre-pulse inhibition, and fear conditioning.

Developmental milestones

Developmental milestones were measured on PND 2, 4, 6, 8, 10, and 12, as previously[44,68]. All measures were conducted by an experimenter blind to genotype. Body weight, length (nose to edge of tail), and head width were measured using a scale (grams) and a digital caliper (cm). Cliff avoidance was tested by placing each pup near the edge of a cardboard box, gently nudging it towards the edge, and measuring the time for it to turn and back away from the edge. Failures to avoid the cliff was recorded as a maximum score of 30-s. Righting reflex was tested by placing each pup on its back, releasing it, and measuring the time for it to fully flip over onto four paws on each developmental day. Negative geotaxis was tested by placing each pup, facing downwards, on a screen angled at 45° from parallel, and measuring the time for it to completely turn and to climb to the top of the screen. Failures to turn and climb were recorded as a maximum score of 30-s. Circle transverse was tested by placing each pup in the center of a circle with a 5″ (12.5 cm) diameter drawn on a laminated sheet of 8.5″ x 11″ white paper, and measuring the time for it to exit the circle. Failures to exit the circle were recorded as a maximum score of 30-s.

Elevated-plus maze

The assay was performed using a mouse EPM (model ENV-560A) purchased from Med Associates (St. Albans, VT) and performed as previously described[69]. The EPM

contained two open arms (35.5 cm x 6 cm) and two closed arms (35.5 cm x 6 cm) radiating from a central area (6 cm x 6 cm). The maze was cleaned with 70% ethanol before the beginning of the first test session and after each subject mouse was tested with sufficient time for the ethanol odor to dissipate before the start of the next test session. Room illumination was ~30 lx.

Light↔dark conflict

The light↔dark assay was performed in accordance with previously described procedures[69]. The test began by placing the mouse in the light side (~320 lx; 28 cm x 27.5 cm x 27 cm) of an automated 2-chambered apparatus, in which the enclosed/dark side (~5 lx; 28 cm x 27.5 cm x 19 cm) was reached by traversing the small opening of the partition between the two chambers. The mouse was allowed to explore freely for 10-min. Time in the dark side chamber and total number of transitions between the light and dark side chambers were automatically recorded during the 10-min session using Labview 8.5.1 software (National Instruments, Austin, TX).

Open Field

General exploratory locomotion in a novel open field arena was evaluated as previously described[44,63,69]. Briefly, each subject was tested in a VersaMax Animal Activity Monitoring System (Accuscan, Columbus, OH, USA) for 30-min in a ~30 lux testing room. Total distance traversed, horizontal activity, vertical activity, and time spent in the center were automatically measured to assess gross motor abilities in mice. Repeated-measures ANOVA was used to detect differences in horizontal, vertical, total, and center time activity obtained during the open field assay. Multiple comparisons were corrected for using Sidak post hoc methods and F, degrees of freedom, and p-values are reported.

Spontaneous Alternation in a Y-maze

Spontaneous alternation was assayed using methods modified based from previous studies[63] in mice. The Y-shaped apparatus (SIZE) was made of non-reflective matte white finished acrylic (P95 White, Tap Plastics, Sacramento, CA, USA). Subjects were

placed in the middle of the apparatus and transitions between the three arms were scored by an investigator blind to genotype. Mice are placed midway of the start arm, facing the center of the y for an 8 minute test period and the sequence of entries into each arm are recorded via a ceiling mounted camera integrated with behavioral tracking software (Noldus Ethovision). % spontaneous alternation is calculated as the number of triads (entries into each of the 3 different arms of the maze in a sequence of 3 without returning to a previously visited arm) relative to the number of alteration opportunities. One-way ANOVA was used to detect differences in alternation. Multiple comparisons were corrected for using Sidak post hoc methods and F, degrees of freedom, and p-values are reported.

Novel Object Recognition

The novel object recognition test was conducted as previously described[44,45,70] in opaque matte white (P95 White, Tap Plastics, Sacramento, CA, USA) arenas (41 cm l x 41 cm w x 30 cm h). The assay consisted of four sessions: a 30-min habituation session, a second 10-min habituation phase, a 10-min familiarization session, and a 5-min recognition test. On day 1, each subject was habituated to a clean empty arena for 30-min. 24-h later, each subject was returned to the empty arena for an additional 10-min habituation session. The mouse was then removed from testing arena and was placed in a clean temporary holding cage while two identical objects were placed in the arena. Subjects were returned to the testing arena and given a 10-min of familiarization period in which they had time to investigate the two identical objects. After the familiarization phase subjects were returned to their holding cages for a 1-h interval period. One familiar object and one novel object were placed in the arena, where the two identical objects had been located during the familiarization phase. After the 1-h interval, each subject was returned to the arena for a 5-min recognition test. The familiarization session and the recognition test were recorded using Ethovision XT video tracking software (version 9.0, Noldus Information Technologies, Leesburg, VA, USA). Sniffing was defined as head facing the object with the nose point within 2 cm from the object. Time spent sniffing each object was scored by an investigator blind to both genotype and treatment. Recognition memory was evaluated by time spent sniffing the

novel object versus the familiar object and innate side bias was accounted for by comparing sniff time of the two identical objects during familiarization. Within genotype repeated-measures ANOVA was used to analyze novel object recognition using novel versus familiar objects as comparison. F, degrees of freedom, and p-values are reported.

Balance beam walking

Balance beam walking is a standard measure of motor coordination and balance[71,72]. We followed a procedure similar to methods previously described using our behavioral core[73]. Balance beam walking is sensitive to genetic mutations that affect neuromuscular, spinal, cerebellar, and other motor systems. It is a non-invasive and non-stressful assay. The apparatus consists of a start platform, an enclosed finish platform, and dowel suspended between the two platforms. The beam is approximately 8 inches above the table or floor surface. The mouse is motivated to cross the dowel beam to reach the dark, enclosed finish platform. Beams of varying dimensions, including square and round shapes, are interchangeable for attaching to the platforms. Training begins with large beams. Progressively smaller beams are employed as the mouse learns the traversal task. Latency to traverse the length of the beam, number of footslips off the edge of the beam, and falls (if any), are scored by the investigator from coded video recordings. Approximately four trials per day for three days represents a standard training protocol. The investigator is present in the test room throughout the session. The balance beam apparatus is thoroughly cleaned with 70% ethanol between each subject trial and following the conclusion of all testing.

Rotarod

Motor coordination, balance, and motor learning were assessed using an accelerating rotarod (Ugo Basile, Schwenksville, PA) as previously described[74,75]. Mice were placed on a cylinder which slowly accelerated from4 to 40 revolutions perminute over a 5-minute (300-second) test session. The task requires the mice to walk forward in order to remain on top of the rotating cylinder rod. Mice were given 3 trials per day with a 30–60-

minute intertrial rest interval. Mice were tested overtwo consecutive days for a total of 6 trials. Latency to fall was recorded with a 300-second maximum latency.

70% ethanol between each subject trial and following the conclusion of all testing.

Repetitive self-grooming

Spontaneous repetitive self-grooming behavior was scored as previously described[63,69,74,76,77]. Each mouse was placed individually into a standard mouse cage (46 cm long × 23.5 cm wide × 20 cm high). Cages were empty to eliminate digging in the bedding, which is a potentially competing behavior. The room was illuminated at ~40 lx. A front-mounted CCTV camera (Security Cameras Direct) was placed ~1 m from the cages to record the sessions. Sessions were videotaped for 20 min. The first 10-min period was habituation and was unscored. Each subject was scored for cumulative time spent grooming all the body regions during the second 10 min of the test session.

Three chambered social approach

Social approach was tested in an automated three-chambered apparatus using methods similar to those previously described[44,63,69,77,78]. Automated Ethovision XT videotracking software (Version 9.0, Noldus Information Technologies, Leesburg, VA) and modified nonreflective materials for the chambers were employed to maximize throughput. The updated apparatus (40 cm × 60 cm × 23 cm) was a rectangular, three-chambered box made from matte white finished acrylic (P95 White, Tap Plastics, Sacramento, CA). Opaque retractable doors (12 cm × 33 cm) were designed to create optimal entryways between chambers (5 cm × 10 cm), while providing maximal manual division of compartments. Three zones, defined using the EthoVision XT software, detected time in each chamber for each phase of the assay. Zones were defined as the annulus extending 2 cm from each novel object or novel mouse enclosure (inverted wire cup, Galaxy Cup, Kitchen Plus, https://www.spectrumdiversified.com/whs/products/Galaxy-Pencil-Utility-Cup). Direction of the head, facing toward the cup enclosure, defined sniff time. A top-mounted infrared-sensitive camera (Ikegami ICD-49, B&H Photo, New York, NY) was positioned directly

above every pair of three-chambered units. Infrared lighting (Nightvisionexperts.com) provided uniform, low-level illumination. The subject mouse was first contained in the center chamber for 10 min, then allowed to explore all three empty chambers during a 10 min habituation session, then allowed to explore the three chambers containing a novel object in one side chamber and a novel mouse in the other side chamber. Lack of innate side preference was confirmed during the initial 10 min of habituation to the entire arena. Novel stimulus mice were 129Sv/ImJ, a relatively inactive strain, aged 10–14 weeks, and matched to the subject mice by sex. Number of entries into the side chambers served as a within-task control for levels of general exploratory locomotion.

Male-female social interaction

The male–female reciprocal social interaction test was conducted as previously described[63,69,74,76,77]. Briefly, each freely moving male subject was paired for 5-min with a freely moving unfamiliar estrous WT female. A closed-circuit television camera (Panasonic, Secaucus, NJ) was positioned at an angle from the Noldus PhenoTyper arena (Noldus, Leesburg, VA) for optimal video quality. An ultrasonic microphone (Avisoft UltraSoundGate condenser microphone capsule CM15; Avisoft Bioacoustics, Berlin, Germany) was mounted 20 cm above the cage. Sampling frequency for the microphone was 250 kHz, and the resolution was 16 bits. The entire apparatus was contained in a sound-attenuating environmental chamber (Lafayette Instruments, Lafayette, IN) under dim LED illumination (~10 lx). Duration of nose-to-nose sniffing, nose-to-anogenital sniffing and following were scored using Noldus Observer 8.0XT event recording software (Noldus, Leesburg, VA) as previously described49. Ultrasonic vocalization spectrograms were displayed using Avisoft software and calls were identified manually by a highly trained investigator blinded to genotype.

Fear conditioning

Delay contextual and cued fear conditioning was conducted using an automated fear-conditioning chamber (Med Associates, St Albans, VT, USA) as previously described[44,63,69]. The conditioning chamber (32 × 25 × 23 cm3, Med Associates) interfaced with a PC installed with VideoFreeze software (version 1.12.0.0, Med

Associates) and enclosed in a sound-attenuating cubicle. Training consisted of a 2-min acclimation period followed by three tone–shock (CS–US) pairings (80-dB tone, duration 30 s; 0.5-mA footshock, duration 1 s; intershock interval, 90 s) and a 2.5-min period during which no stimuli were presented. The environment was well lit (~100 lx), with a stainless steel grid floor and swabbed with vanilla odor cue (prepared from vanilla extract; McCormick; 1:100 dilution). A 5-min test of contextual fear conditioning was performed 24 h after training, in the absence of the tone and footshock but in the presence of 100 lx overhead lighting, vanilla odor and chamber cues identical to those used on the training day. Cued fear conditioning, conducted 48 h after training, was assessed in a novel environment with distinct visual, tactile and olfactory cues. Overhead lighting was turned off. The cued test consisted of a 3-min acclimation period followed by a 3-min presentation of the tone CS and a 90-s exploration period. Cumulative time spent freezing in each condition was quantified by VideoFreeze software (Med Associates).

Acoustic Startle and Prepulse inhibition

Subjects were tested in San Diego Instruments startle chambers using standard methods as described previously[74,79]. Test sessions began by placing the mouse in the Plexiglas holding cylinder for a 5 min acclimation period. For the next 8 min, mice were presented with each of six trial types across six discrete blocks of trials, for a total of 36 trials. The intertrial interval was 10–20 s. One trial type measured the response to no stimulus (baseline movement). The other five trial types measured startle responses to 40 ms sound bursts of 80, 90, 100, 110, or 120 dB. The six trial types were presented in pseudorandom order such that each trial type was presented once within a block of six trials. Startle amplitude was measured every 1 ms over a 65ms period beginning at the onset of the startle stimulus. The maximum startle amplitude over this sampling period was taken as the dependent variable. Background noise level of 70 dB was maintained over the duration of the test session. For prepulse inhibition of acoustic startle, mice were presented with each of seven trial types across six discrete blocks of trials for a total of 42 trials, over 10.5 min. The intertrial interval was 10–20 s. One trial type measured the response to no stimulus (baseline movement) and another measured the

startle response to a 40 ms, 110 dB sound burst. The other five trial types were acoustic prepulse stimulus plus acoustic startle stimulus trials. The seven trial types were presented in pseudorandom order such that each trial type was presented once within a block of seven trials. Prepulse stimuli were 20 ms tones of 74, 78, 82, 86, and 92 dB intensity, presented 100 ms before the 110 dB startle stimulus. Startle amplitude was measured every 1 ms over a 65 ms period, beginning at the onset of the startle stimulus. The maximum startle amplitude over this sampling period was taken as the dependent variable. A background noise level of 70 dB was maintained over the duration of the test session.

Seizure Susceptibility Following Administration of Pentylenetetrazole

Subjects were weighed then administered pentylenetetrazole (80 mg/kg) intraperitoneally. Dosing was conducted in the morning (9:00 -12:00) in a dim (~30 lux) empty holding room. Directly after administration of the convulsant, subjects were placed in a clean, empty cage and subsequent seizure stages were live-scored for 30-min. Seizure stages were scored using latencies to (1) first jerk/Straub's tail, (2) loss of righting, (3) generalized clonic-tonic seizure, and (4) death. Time to each stage was taken in seconds and compared by genotype. One-way ANOVA was used to analyze latencies to first jerk, loss of righting, generalized clonic-tonic seizure, and death. F, degrees of freedom, and p-values are reported.

EEG acquisition

EEG data was acquired using Ponemah (Data Sciences International, St. Paul, MN, USA) and subsequently analyzed using the Neuroscore automated software (Data Sciences International, St. Paul, MN, USA). Subjects were recorded for 24-h baseline in their home cage before administration of 80 mg/kg pentylenetetrazole (Sigma Aldrich, St. Louis, MO, USA) injected intraperitoneally. EEG and EMG were continuously sampled at 500 Hz. Spiking was defined as activity above an absolute threshold of 200 µV-1000 µV that lasted between 0.5 and 100 ms, while spike trains had a minimum duration of 0.5s, a minimum spike interval of 0.05s and a minimum of 4 consecutive spikes. Power spectral densities were determined using a periodogram transformation

from amplitude to frequency domains then log transformed for clearer data illustration. Latency to seizure onset and subsequent death following administration of PTZ was first quantified by observed latencies then confirmed by spectral EEG and amplitude response read-outs. One-way ANOVA was used to analyze bouts of spike train activity and latency to seizure onset and death between genotypes. An overall ANOVA was used to detect a genotype difference across power bands, then genotype differences were analyzed within power bands using multiple comparisons.

Luciferase assay

We constructed luciferase reporter plasmids by cloning an ~900 bp region containing human 1b[30] into the pGL4.24 vector (Promega) upstream of the minP, primers in Table 3. HEK293 cells or SK-N-SH cells (40%–60% confluent) were transfected using Lipofectamine 3000 with each construct (400 ng) and the Renilla luciferase expression vector pRL-TK (40 ng; Promega) in triplicate. After 24 hours, the luciferase activity in the cell lysates was determined using the Dual Luciferase Reporter System (Promega). Firefly luciferase activities were normalized to that of Renilla luciferase, and expression relative to the activity of an inactive region of noncoding DNA (NEG2) was noted.

Target	**Sequence (5'-3')**
human 1b	F-ttaattaagagctcCGGAAATCATTGCCCCTTCC
	R-ttaattaactcgagAATCTGGATTGTGAGAAAGTGTTT
Human NEG2	F-ccggagctcTGGTATGGGTGAAAACGGCT
	R-cggctcgagGAGGTTTGTGGGGAGGAGTG

Table 3: Primers for cloning regions from human DNA.

CRISPR/dCas9 in HEK293 cells

HEK293 cells were transfected with 500 ng of equimolar pooled SCN1A_h1b sgRNAs (Table 4) and 500 ng dCas9^{p300Core} (Addgene, plasmid #61357) using Lipofectamine 3000. After 24 hours media was refreshed. 48 hours following transfection RNA was collected using RNAqueous kit (Ambion) and cDNA was generated using Superscript III reverse transcriptase (Invitrogen). Changes in gene expression were quantified via qPCR using SYBR green, primers are listed in Table 2.

Target	**Sequence (5'-3')**	**Location (hg19)**
h1b_1	GCTATTTGCTGATTTGTATTAGG	Chr2: 166128022 166128044
h1b_2	GAGGATACTGCAGAGGTCTCTGG	Chr 2: 166984479-166984501
h1b_3	GGAAGGTTGAGAGAGGAGGGGGG	Chr 2: 166984086-166984108
h1b_4	AGTATCTGCAGTATCATTGCTGG	Chr 2: 166983556 166983578
h1b_5	GGAAAATTCCATGCTGAGGTTGG	Chr 2: 166983037 166983059
h1b_6	TGAATGGCCACAGAGATTTACGG	Chr 2: 166982669 166982691

Table 4: sgRNA sequences for CRISPR dCas9 induction.

References

1. Landry, J.-R., Mager, D. L. & Wilhelm, B. T. Complex controls: the role of alternative promoters in mammalian genomes. *Trends Genet.* **19**, 640–8 (2003).

2. Forrest, A. R. R. *et al.* A promoter-level mammalian expression atlas. *Nature* **507**, 462–470 (2014).

3. Carninci, P. *et al.* The transcriptional landscape of the mammalian genome. *Science* **309**, 1559–63 (2005).

4. Yamashita, R. *et al.* Genome-wide characterization of transcriptional start sites in humans by integrative transcriptome analysis. *Genome Res.* **21**, 775–89 (2011).

5. Davuluri, R. V., Suzuki, Y., Sugano, S., Plass, C. & Huang, T. H. M. The functional consequences of alternative promoter use in mammalian genomes. *Trends in Genetics* **24**, 167–177 (2008).

6. Kimura, K. *et al.* Diversification of transcriptional modulation: large-scale identification and characterization of putative alternative promoters of human genes. *Genome Res.* **16**, 55–65 (2006).

7. de Klerk, E. & ’t Hoen, P. A. C. Alternative mRNA transcription, processing, and translation: insights from RNA sequencing. *Trends Genet.* **31**, 128–39 (2015).

8. Tzvetkov, M. V., Meineke, C., Oetjen, E., Hirsch-Ernst, K. & Brockmöller, J. Tissue-specific alternative promoters of the serotonin receptor gene HTR3B in human brain and intestine. *Gene* **386**, 52–62 (2007).

9. Reyes, A. & Huber, W. Alternative start and termination sites of transcription drive most transcript isoform differences across human tissues. *Nucleic Acids Res.* **46**, 582–592 (2018).

10. Kim, T. H. *et al.* A high-resolution map of active promoters in the human genome. *Nature* **436**, 876–80 (2005).

11. Sandelin, A. *et al.* Mammalian RNA polymerase II core promoters: insights from genome-wide studies. *Nat. Rev. Genet.* **8**, 424–36 (2007).

12. Karlsson, K., Lönnerberg, P. & Linnarsson, S. Alternative TSSs are co-regulated in single cells in the mouse brain. *Mol. Syst. Biol.* **13**, 930 (2017).

13. Li, G. *et al.* Extensive promoter-centered chromatin interactions provide a topological basis for transcription regulation. *Cell* **148**, 84–98 (2012).

14. Zhang, Y. *et al.* Chromatin connectivity maps reveal dynamic promoter–enhancer long-range associations. *Nature* **504**, 306–310 (2013).

15. Claes, L. R. *et al.* The *SCN1A* variant database: a novel research and diagnostic tool. *Hum. Mutat.* **30**, E904–E920 (2009).

16. Lossin, C. A catalog of SCN1A variants. *Brain Dev.* **31**, 114–130 (2009).

17. Parihar, R. & Ganesh, S. The SCN1A gene variants and epileptic encephalopathies. *J. Hum. Genet.* **58**, 573–580 (2013).

18. McArdle, E. J., Kunic, J. D., George, A. L. & Jr. Novel SCN1A frameshift mutation with absence of truncated Nav1.1 protein in severe myoclonic epilepsy of infancy. *Am. J. Med. Genet. A* **146A**, 2421–3 (2008).

19. Meng, H. *et al.* The SCN1A mutation database: updating information and analysis of the relationships among genotype, functional alteration, and phenotype. *Hum. Mutat.* **36**, 573–80 (2015).

20. Yu, F. H. *et al.* Reduced sodium current in GABAergic interneurons in a mouse model of severe myoclonic epilepsy in infancy. *Nat. Neurosci.* **9**, 1142–1149 (2006).

21. Ogiwara, I. *et al.* Nav1.1 haploinsufficiency in excitatory neurons ameliorates seizure-associated sudden death in a mouse model of Dravet syndrome. *Hum. Mol. Genet.* **22**, 4784–804 (2013).

22. Miller, A. R., Hawkins, N. A., McCollom, C. E. & Kearney, J. A. Mapping genetic modifiers of survival in a mouse model of Dravet syndrome. *Genes. Brain. Behav.* **13**, 163–72 (2014).

23. Tai, C., Abe, Y., Westenbroek, R. E., Scheuer, T. & Catterall, W. A. Impaired excitability of somatostatin- and parvalbumin-expressing cortical interneurons in a mouse model of Dravet syndrome. *Proc. Natl. Acad. Sci.* **111**, E3139–E3148 (2014).

24. Dutton, S. B. *et al.* Preferential inactivation of Scn1a in parvalbumin interneurons increases seizure susceptibility. *Neurobiol. Dis.* **49**, 211–20 (2013).

25. Cheah, C. S. *et al.* Specific deletion of NaV1.1 sodium channels in inhibitory interneurons causes seizures and premature death in a mouse model of Dravet syndrome. *Proc. Natl. Acad. Sci. U. S. A.* **109**, 14646–51 (2012).

26. Ogiwara, I. *et al.* Nav1.1 Localizes to Axons of Parvalbumin-Positive Inhibitory Interneurons: A Circuit Basis for Epileptic Seizures in Mice Carrying an Scn1a Gene Mutation. *J. Neurosci.* **27**, 5903–5914 (2007).

27. Kalume, F. Sudden unexpected death in Dravet syndrome: Respiratory and other physiological dysfunctions. *Respir. Physiol. Neurobiol.* **189**, 324–328 (2013).

28. Shmuely, S., Sisodiya, S. M., Gunning, W. B., Sander, J. W. & Thijs, R. D. Mortality in Dravet syndrome: A review. *Epilepsy Behav.* **64**, 69–74 (2016).

29. Wirrell, E. C. Treatment of Dravet Syndrome. *Can. J. Neurol. Sci. / J. Can. des Sci. Neurol.* **43**, S13–S18 (2016).

30. Martin, M. S., Tang, B., Ta, N. & Escayg, A. Characterization of 5′ untranslated regions of the voltage-gated sodium channels SCN1A, SCN2A, and SCN3A and identification of cis-conserved noncoding sequences. *Genomics* **90**, 225–235 (2007).

31. Long, Y.-S. *et al.* Identification of the promoter region and the 5′-untranslated

exons of the human voltage-gated sodium channel Na_v 1.1 gene (*SCN1A*) and enhancement of gene expression by the 5′-untranslated exons. *J. Neurosci. Res.* **86**, 3375–3381 (2008).

32. International League Against Epilepsy Consortium on Complex Epilepsies. Electronic address: epilepsy-austin@unimelb.edu.au. Genetic determinants of common epilepsies: a meta-analysis of genome-wide association studies. *Lancet Neurol.* **13**, 893–903 (2014).

33. ILAE, T. I. L. A. E. C. on C. E. Genome-wide mega-analysis identifies 16 loci and highlights diverse biological mechanisms in the common epilepsies. *Nat. Commun.* **9**, 5269 (2018).

34. Gao, Q.-W. *et al.* A Point Mutation in SCN1A 5′ Genomic Region Decreases the Promoter Activity and Is Associated with Mild Epilepsy and Seizure Aggravation Induced by Antiepileptic Drug. *Mol. Neurobiol.* **54**, 2428–2434 (2017).

35. Nakayama, T. *et al.* Deletions of SCN1A 5′ genomic region with promoter activity in Dravet syndrome. *Hum. Mutat.* **31**, 820–829 (2010).

36. Lange, I. M. *et al.* Influence of common *SCN1A* promoter variants on the severity of *SCN1A* -related phenotypes. *Mol. Genet. Genomic Med.* e727 (2019). doi:10.1002/mgg3.727

37. Wang, D. *et al.* Comprehensive functional genomic resource and integrative model for the human brain. *Science (80-.).* **362**, eaat8464 (2018).

38. Lonsdale, J. *et al.* The Genotype-Tissue Expression (GTEx) project. *Nat. Genet.* **45**, 580 (2013).

39. Consortium, R. E. *et al.* Integrative analysis of 111 reference human epigenomes. *Nature* **518**, 317 (2015).

40. Fullard, J. F. *et al.* An atlas of chromatin accessibility in the adult human brain. *Genome Res.* **28**, 1243–1252 (2018).

41. Mo, A. *et al.* Epigenomic Signatures of Neuronal Diversity in the Mammalian Brain. *Neuron* **86**, 1369–84 (2015).

42. Cheah, C. S. *et al.* Channels Correlations in timing of sodium channel expression, epilepsy, and sudden death in Dravet syndrome. *Channels* **7**, 468–472

43. Hawkins, N. A., Calhoun, J. D., Huffman, A. M. & Kearney, J. A. Gene expression profiling in a mouse model of Dravet syndrome. *Exp. Neurol.* **311**, 247–256 (2019).

44. Adhikari, A. *et al.* Cognitive deficits in the Snord116 deletion mouse model for Prader-Willi syndrome. *Neurobiol. Learn. Mem.* (2018). doi:10.1016/j.nlm.2018.05.011

45. Flannery, B. M. *et al.* Behavioral assessment of NIH Swiss mice acutely intoxicated with tetramethylenedisulfotetramine. *Neurotoxicol. Teratol.* **47**, 36–45 (2015).

46. Genton, P., Velizarova, R. & Dravet, C. Dravet syndrome: The long-term outcome. *Epilepsia* **52**, 44–49 (2011).

47. Rubinstein, M. *et al.* Dissecting the phenotypes of Dravet syndrome by gene deletion. *Brain* **138**, 2219–2233 (2015).

48. NA Copping, A Adhikari, SP Petkova, and J. S. Genetic Backgrounds Have Unique Seizure Response Profiles and Behavioral Outcomes Following Convulsant Administration. *Epilepsy Behav.* (2019).

49. Featherstone, R. E. *et al.* EEG biomarkers of target engagement, therapeutic effect, and disease process. *Ann. N. Y. Acad. Sci.* **1344**, 12–26 (2015).

50. Modi, M. E. & Sahin, M. Translational use of event-related potentials to assess circuit integrity in ASD. *Nat. Rev. Neurol.* **13**, 160–170 (2017).

51. Dickinson, A. *et al.* Interhemispheric alpha-band hypoconnectivity in children with

autism spectrum disorder. *Behav. Brain Res.* **348**, 227–234 (2018).

52. Cunningham, T. J. *et al.* Genomic Knockout of Two Presumed Forelimb Tbx5 Enhancers Reveals They Are Nonessential for Limb Development. *Cell Rep.* **23**, 3146–3151 (2018).

53. Dickel, D. E. *et al.* Ultraconserved Enhancers Are Required for Normal Development. *Cell* **172**, 491-499.e15 (2018).

54. Hewitt, S. C. *et al.* A distal super enhancer mediates estrogen-dependent mouse uterine-specific gene transcription of Igf1 (insulin-like growth factor 1). *J. Biol. Chem.* **294**, 9746–9759 (2019).

55. Johnson, K. R. *et al.* Deletion of a long-range Dlx5 enhancer disrupts inner ear development in mice. *Genetics* **208**, 1165–1179 (2018).

56. Sidorov, M. S. *et al.* Delta rhythmicity is a reliable EEG biomarker in Angelman syndrome: a parallel mouse and human analysis. *J. Neurodev. Disord.* **9**, 17 (2017).

57. Frohlich, J. *et al.* Mechanisms underlying the EEG biomarker in Dup15q syndrome. *Mol. Autism* **10**, 29 (2019).

58. Frohlich, J. *et al.* A Quantitative Electrophysiological Biomarker of Duplication 15q11.2-q13.1 Syndrome. *PLoS One* **11**, e0167179 (2016).

59. Marquardt, K., Sigdel, R. & Brigman, J. L. Touch-screen visual reversal learning is mediated by value encoding and signal propagation in the orbitofrontal cortex. *Neurobiol. Learn. Mem.* **139**, 179–188 (2017).

60. Guerrini, R. *et al.* Lamotrigine and seizure aggravation in severe myoclonic epilepsy. *Epilepsia* **39**, 508–12 (1998).

61. Matharu, N. *et al.* CRISPR-mediated activation of a promoter or enhancer rescues obesity caused by haploinsufficiency. *Science (80-.).* **363**, eaau0629 (2019).

62. Mali, P. *et al.* RNA-guided human genome engineering via Cas9. *Science (80-.).* **339**, 823–826 (2013).

63. Gompers, A. L. *et al.* Germline Chd8 haploinsufficiency alters brain development in mouse. *Nat. Neurosci.* **20**, 1062–1073 (2017).

64. Dobin, A. *et al.* STAR: ultrafast universal RNA-seq aligner. *Bioinformatics* **29**, 15–21 (2013).

65. Liao, Y., Smyth, G. K. & Shi, W. FeatureCounts: An efficient general purpose program for assigning sequence reads to genomic features. *Bioinformatics* **30**, 923–930 (2014).

66. Wang, L., Wang, S. & Li, W. RSeQC: quality control of RNA-seq experiments. *Bioinformatics* **28**, 2184–5 (2012).

67. MD, R., DJ, M. & GK, S. edgeR: a Bioconductor package for differential expression analysis of digital gene expression data. *Bioinformatics* **26**, 139–40 (2009).

68. Fox, W. M. Reflex-ontogeny and behavioural development of the mouse. *Anim. Behav.* **13**, 234-IN5 (1965).

69. Copping, N. A. *et al.* Neuronal overexpression of Ube3a isoform 2 causes behavioral impairments and neuroanatomical pathology relevant to 15q11.2-q13.3 duplication syndrome. *Hum. Mol. Genet.* **26**, 3995–4010 (2017).

70. Yang, M., Lewis, F. C., Sarvi, M. S., Foley, G. M. & Crawley, J. N. 16p11.2 Deletion mice display cognitive deficits in touchscreen learning and novelty recognition tasks. *Learn. Mem.* **22**, 622–32 (2015).

71. Brooks, S. P., Pask, T., Jones, L. & Dunnett, S. B. Behavioural profiles of inbred mouse strains used as transgenic backgrounds. I: motor tests. *Genes. Brain. Behav.* **3**, 206–15 (2004).

72. Carter, R. J., Morton, J. & Dunnett, S. B. Motor Coordination and Balance in Rodents. *Curr. Protoc. Neurosci.* **15**, 8.12.1-8.12.14 (2001).

73. Vogel Ciernia, A. *et al.* Early motor phenotype detection in a female mouse model of Rett syndrome is improved by cross-fostering. *Hum. Mol. Genet.* **26**, 1839–1854 (2017).

74. Yang, M. *et al.* Reduced excitatory neurotransmission and mild autism-relevant phenotypes in adolescent Shank3 null mutant mice. *J. Neurosci.* **32**, 6525–41 (2012).

75. Silverman, J. L. *et al.* Sociability and motor functions in Shank1 mutant mice. *Brain Res.* **1380**, 120–37 (2011).

76. Silverman, J. L. *et al.* GABAB Receptor Agonist R-Baclofen Reverses Social Deficits and Reduces Repetitive Behavior in Two Mouse Models of Autism. *Neuropsychopharmacology* **40**, 2228–39 (2015).

77. Dhamne, S. C. *et al.* Replicable in vivo physiological and behavioral phenotypes of the Shank3B null mutant mouse model of autism. *Mol. Autism* **8**, 26 (2017).

78. Copping, N. A. *et al.* Touchscreen learning deficits and normal social approach behavior in the Shank3B model of Phelan–McDermid Syndrome and autism. *Neuroscience* **345**, 155–165 (2017).

79. Papaleo, F. *et al.* Working memory deficits, increased anxiety-like traits, and seizure susceptibility in BDNF overexpressing mice. *Learn. Mem.* **18**, 534–44 (2011).

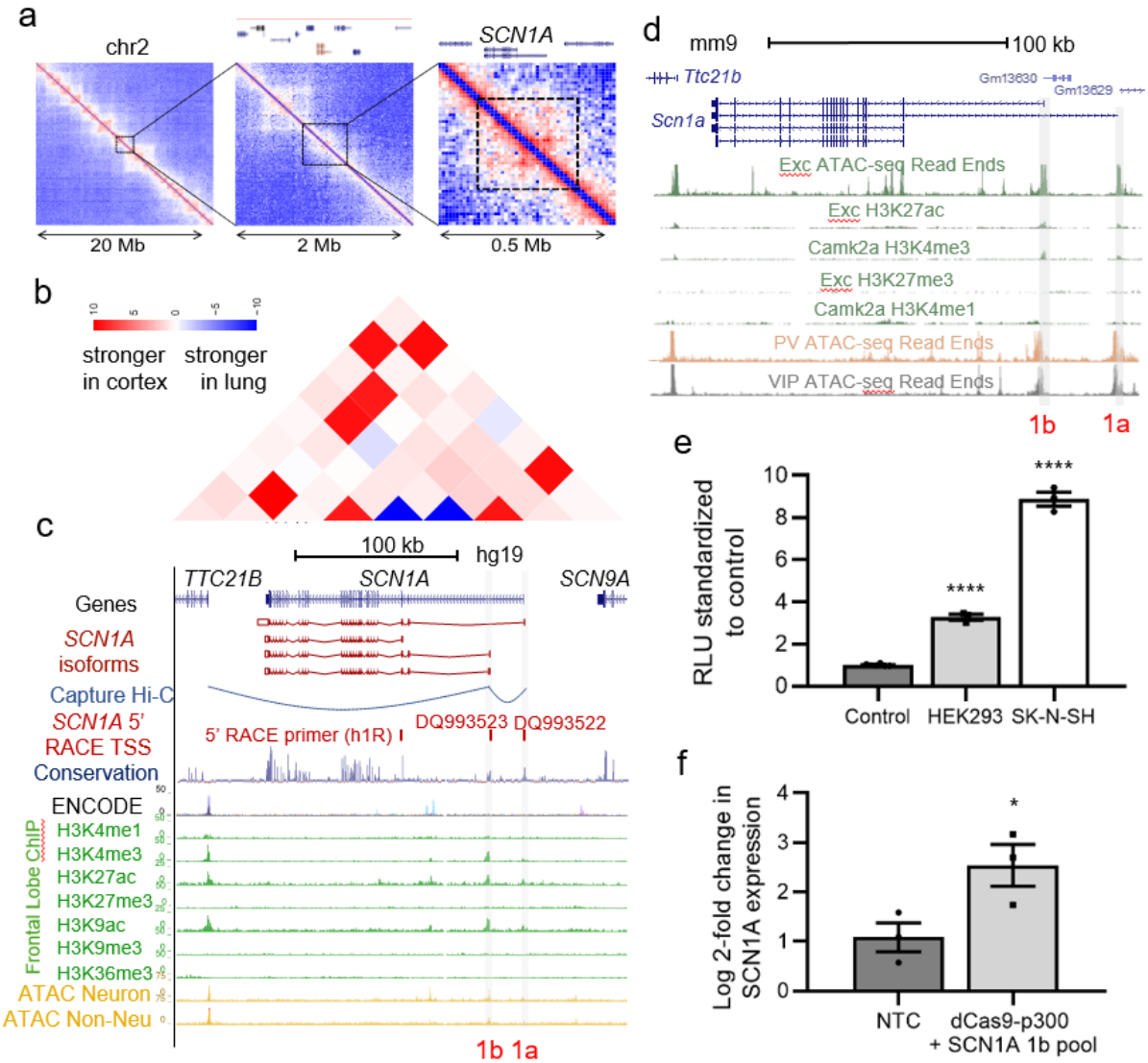

Figure 1 – Genomic context of *SCN1A* gene showing chromatin conformation information. (a) Hi-C contact heatmaps showing chromosomal neighborhood of *SCN1A* at different ranges. (b) Contrasting differential Hi-C contact heatmaps showing differences between PFC and lung. (c) Human (hg19) *SCN1A* locus showing signal for histone PTMs and ATAC-seq for neuronal and non-neuronal cells derived from dorsolateral PFC. (d) Mouse (mm10) *Scn1a* locus showing signal for histone PTMs and ATAC-seq for neuronal cell types. (e) Activity of human 1b region in luciferase assay with minimal promoter in HEK293 (****P < 0.0001) and SK-N-SH cells (****P < 0.0001) shown as mean ± SEM. (d) Transcriptional activation of *SCN1A* using gRNAs targeting 1b co-transfected with dCas9-p300 in HEK293 cells increases *SCN1A* expression (*P = 0.047) when compared to empty vector (EV) as measured by qPCR and normalized to non-transfected control, shown as mean ± SEM. For panels a through e, see text for data sources.

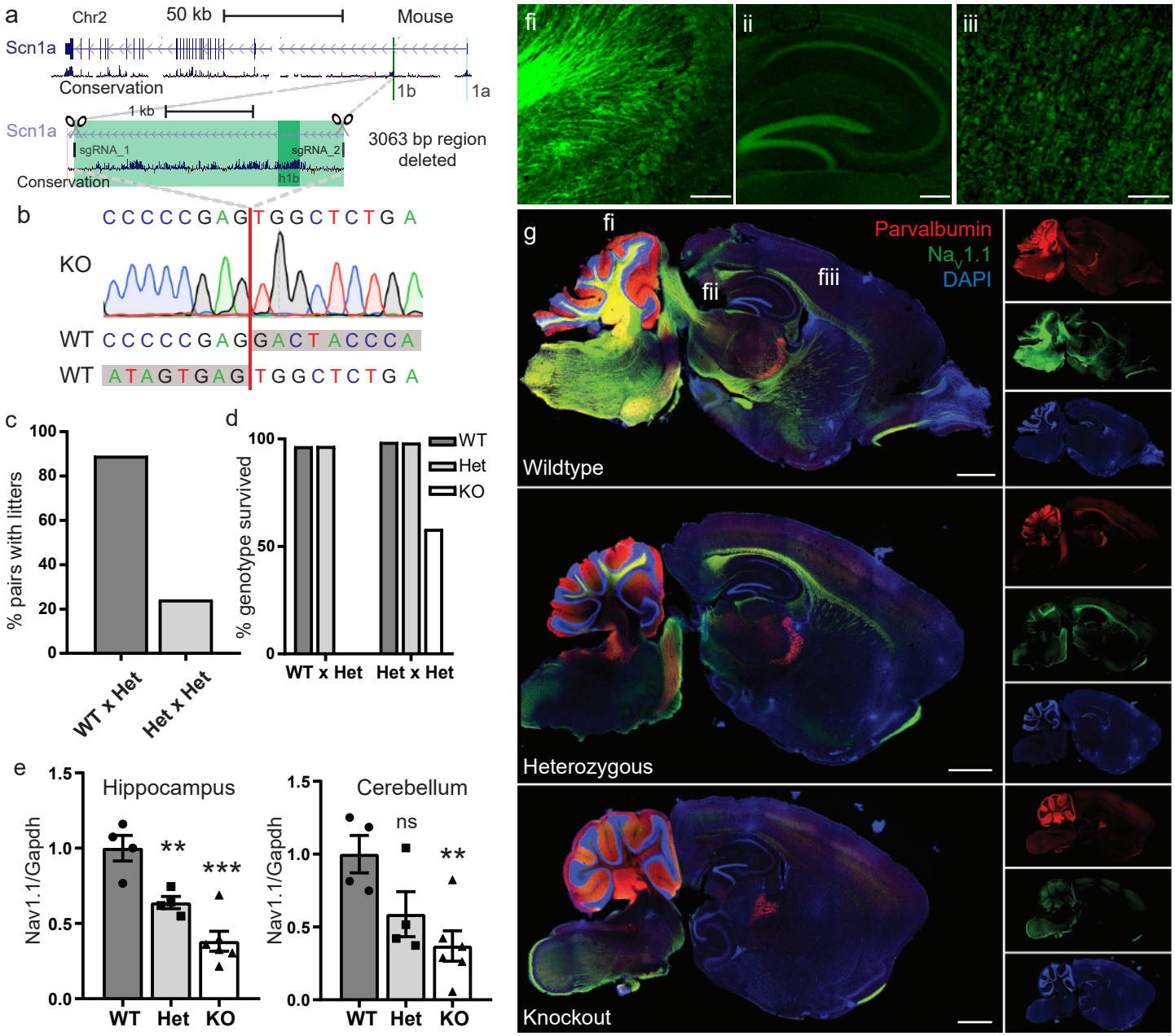

Figure 2: Scn1a 1b deletion mouse model. (a) Location of 1a and 1b regions at mouse Scn1a locus showing guideRNA sequence targets for Cas9-directed deletion of mouse 1b removal of entire 3063 bp conserved region. (b) Sequence trace validating deleted region. (c) Proportion of pairings that produced a litter in either WT x Het or Het x Het matings. (d) Proportion of mice from each genotype that survived from either WT x Het or Het x Het matings. (e) Western blots of adult mouse brain regional lysates, showing reduction of NaV1.1 protein in hippocampus of Het (**P = 0.016) and KO (***P = 0.001) mice (WT n = 4, Het n = 4, KO n = 6) and cerebellum of Het (P = 0.087) and KO (**P = 0.007) mice (WT n = 4, het n = 4, KO n = 6).
(f) Immunofluorescent analysis of NaV1.1 in wildtype mice across cerebellum (i), hippocampus (ii) and cortex (iii), regions taken from wildtype in panel f. Scale bars i and ii = 100 µm, ii = 250 µm.
(g) Immunofluorescent analysis of sagittal sections of P28 mice revealed a reduction in NaV1.1 (green) expression in homozygous versus WT mice with no changes in parvalbumin (red) expression. Scale bars = 1 mm.

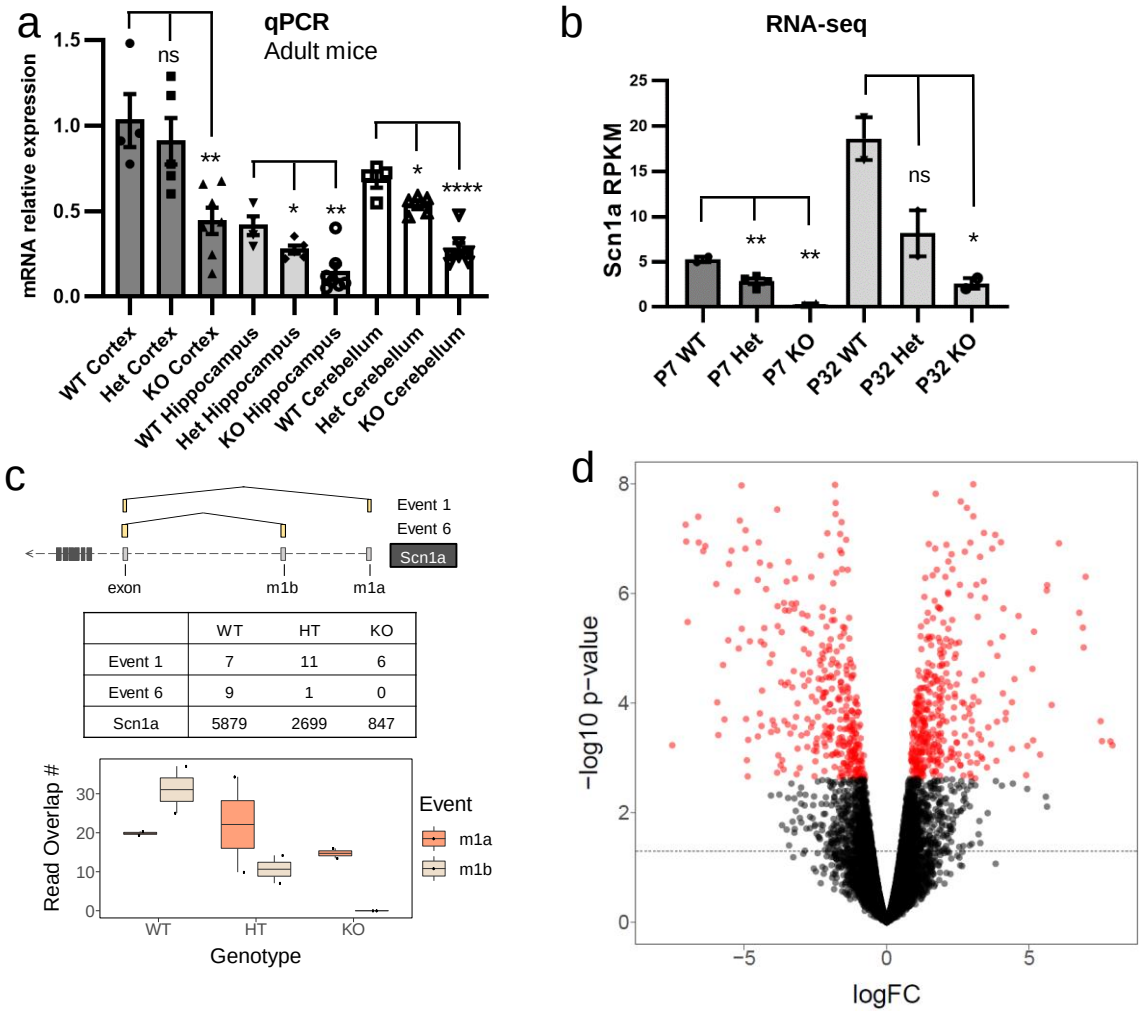

	WT	HT	KO
Event 1	7	11	6
Event 6	9	1	0
Scn1a	5879	2699	847

e

Catergory	#DE	Total	Term	Ontology	FDR
GO:0031226	70	1037	intrinsic component of plasma membrane	CC	2.36E-09
GO:0007411	26	211	axon guidance	BP	1.22E-07
GO:0000902	55	960	cell morphogenesis	BP	1.55E-05
GO:0022008	74	1505	neurogenesis	BP	2.66E-05
GO:0048666	57	1070	neuron development	BP	7.22E-05
GO:0030182	62	1269	neuron differentiation	BP	0.000345
GO:0030001	45	666	metal ion transport	BP	6.93E-07
GO:0050890	25	283	cognition	BP	4.37E-05
GO:0044456	52	998	synapse part	CC	7.41E-05
GO:0007267	59	1228	cell-cell signaling	BP	0.000107
GO:0099536	39	640	synaptic signaling	BP	0.000107
GO:0007600	26	355	sensory perception	BP	0.000178

Figure 3: Differential gene expression with *Scn1a* 1b deletion. (a) Bar plot showing relative expression of *Scn1a* using qPCR in 3-month-old mice (mean ± SEM), values normalized to WT cortex. *Scn1a* expression reduced in KO cortex vs WT cortex (**P = 0.0040), Het hippocampus vs WT hippocampus (*P = 0.0399), KO hippocampus vs WT hippocampus (**P = 0.0055), Het cerebellum vs WT cerebellum (*P = 0.0196) and KO cerebellum vs WT cerebellum (****P < 0.0001). (b) Bar plot indicating logRPKM *Scn1a* expression between WT and Het or KO mutants in postnatal day (P) 7 forebrain or P32 hippocampus, (mean ± SEM). *Scn1a* expression reduced in P7 Het (**P = 0.0095) and KO (**P = 0.0039) and P32 KO (*P = 0.0224) versus wildtype. (c, top) Schematic showing splicing of m1a, m1b, and m1c sequences with first *Scn1a* coding exon in reference. Events 2-5 are shown in the supplement. (c, middle) Table showing the number of sequencing reads that overlap each splicing event and the entire *Scn1a* locus for WT, heterozygous, and homozygous 1b null mice. The full table is included in the supplement. (c, bottom) Bar plot indicating the number of sequencing reads with alignment overlapping the m1a, m1b, or m1c locus for each genotype along the x-axis. (d) Scatterplot of differentially-expressed genes in homozygous null mice. Genes with p-value < 0.05 are in red. (e) Table showing select pathways enriched in differentially-expressed genes for knockout mice. Pathways enriched in up-regulated genes are shown in the peach color. Pathways enriched in down-regulated genes are shown in blue. Pathways shown have 300 or fewer genes annotated to the category. Ontologies are biological pathways (BP), molecular function (MF), or cellular component (CC).

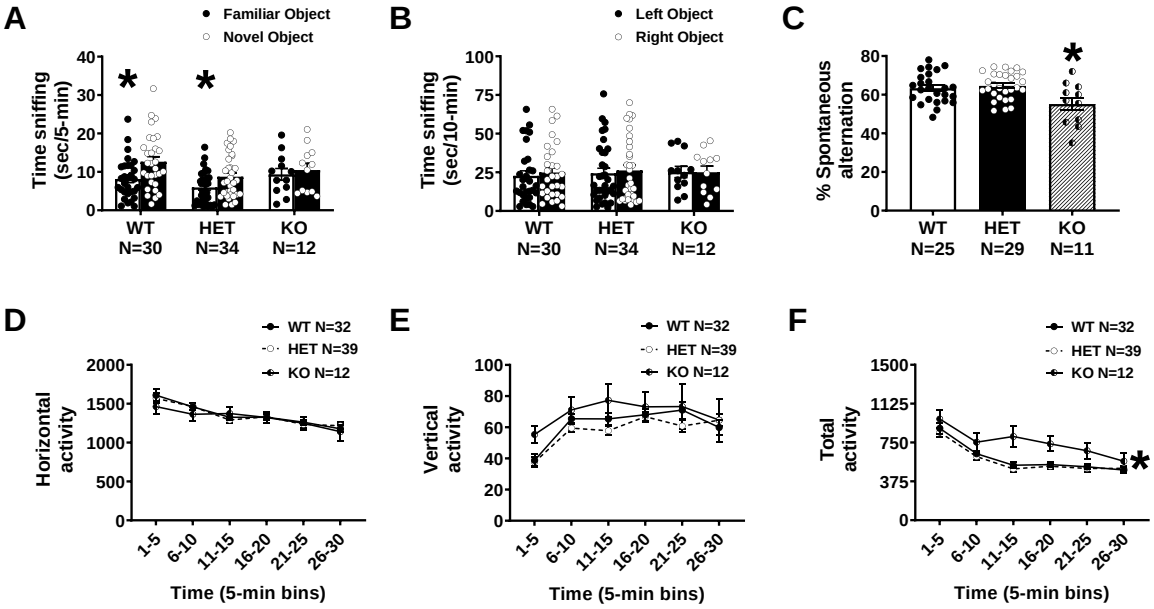

Figure 4: *Scn1a* 1b homozygous deletion mice exhibit learning and memory impairments without confounds in gross motor abilities. Recognition memory was assessed using a novel object recognition assay. (a) 1b KO mice did not spend more time sniffing the novel object over the familiar object. 1b Het and WT performed with typical preference. (b) All genotypes showed no preference for either the left or right object during the familiarization phase indicating no innate side bias confounds in the novel object recognition trials. *, $p < 0.05$, repeated-measures ANOVA within genotype using the familiar versus novel object for comparison. (c) Working memory impairments were observed by lower percentages of spontaneous alternation in the Y-Maze. *, $p < 0.05$, One-way ANOVA. (d) No genotype differences in horizontal (d) or (e) vertical activity counts in the 1b Het and KO mice compared to their wildtype littermate controls. (f) KO 1b deletion mice were hyperactive in total activity during two different 5-min bins of the 30-min assay. Moreover, when total activity is summed and re-graphed as a bar graph, comparisons between KO versus WT and Het in total movement were observed. Analyses include both males and females. *$p < 0.05$, repeated measures ANOVA, main effect of genotype.

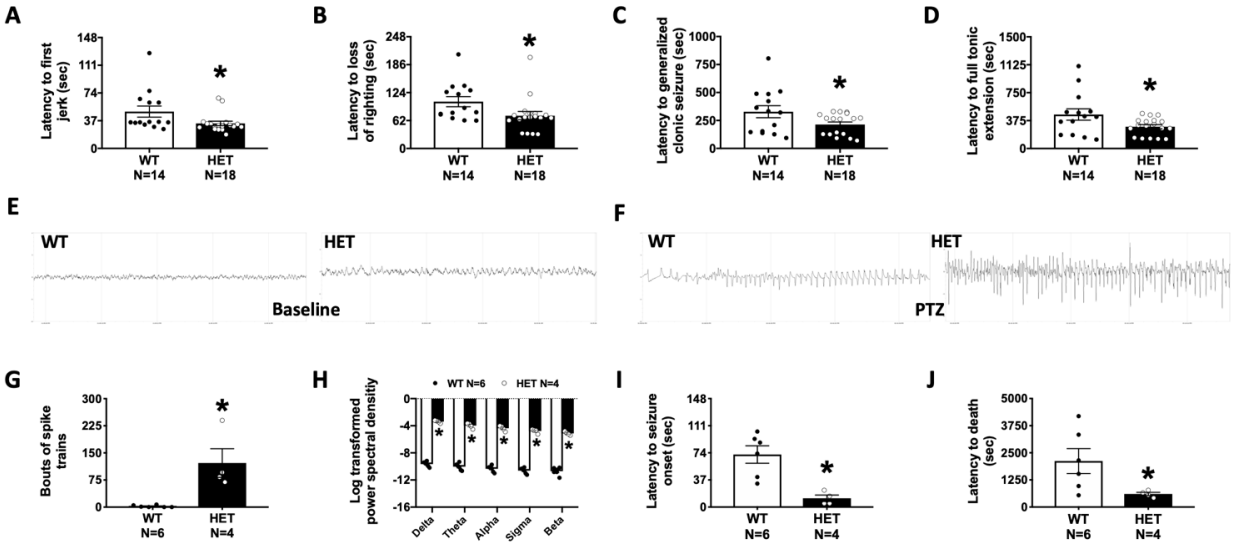

Figure 5: Increased seizure susceptibility and abnormal EEG in heterozygous 1b deletion mice. (a-d) Latency measures were observed after an i.p. injection of 80 mg/kg PTZ over the course of a 30-min trial. Reduced latencies to first jerk, loss of righting, generalized clonic seizure, and full tonic extension were observed in Het mice when compared to WT littermate controls. EEG was collected using a wireless telemetry system before and after an i.p. injection of 80 mg/kg PTZ. **(e-f)** Representative EEG traces of WT and Het mice during baseline EEG recording and subsequent PTZ response. Powerband calculations and spiking events were automatically scored. **(g)** Het mice had significantly more spiking events and spike trains during baseline EEG acquisition when compared to WT. **(h)** Het mice also had significantly higher power across all frequency bins, Delta (0-4 Hz), Theta (4-8 Hz), Alpha (8-12 Hz), Sigma (12-16 Hz), and Beta (16-30) during baseline when compared to controls. Finally, seizure susceptibility was confirmed with EEG after PTZ administration. **(i-j)** Reduced latencies to seizure onset and death were observed in Het mice.

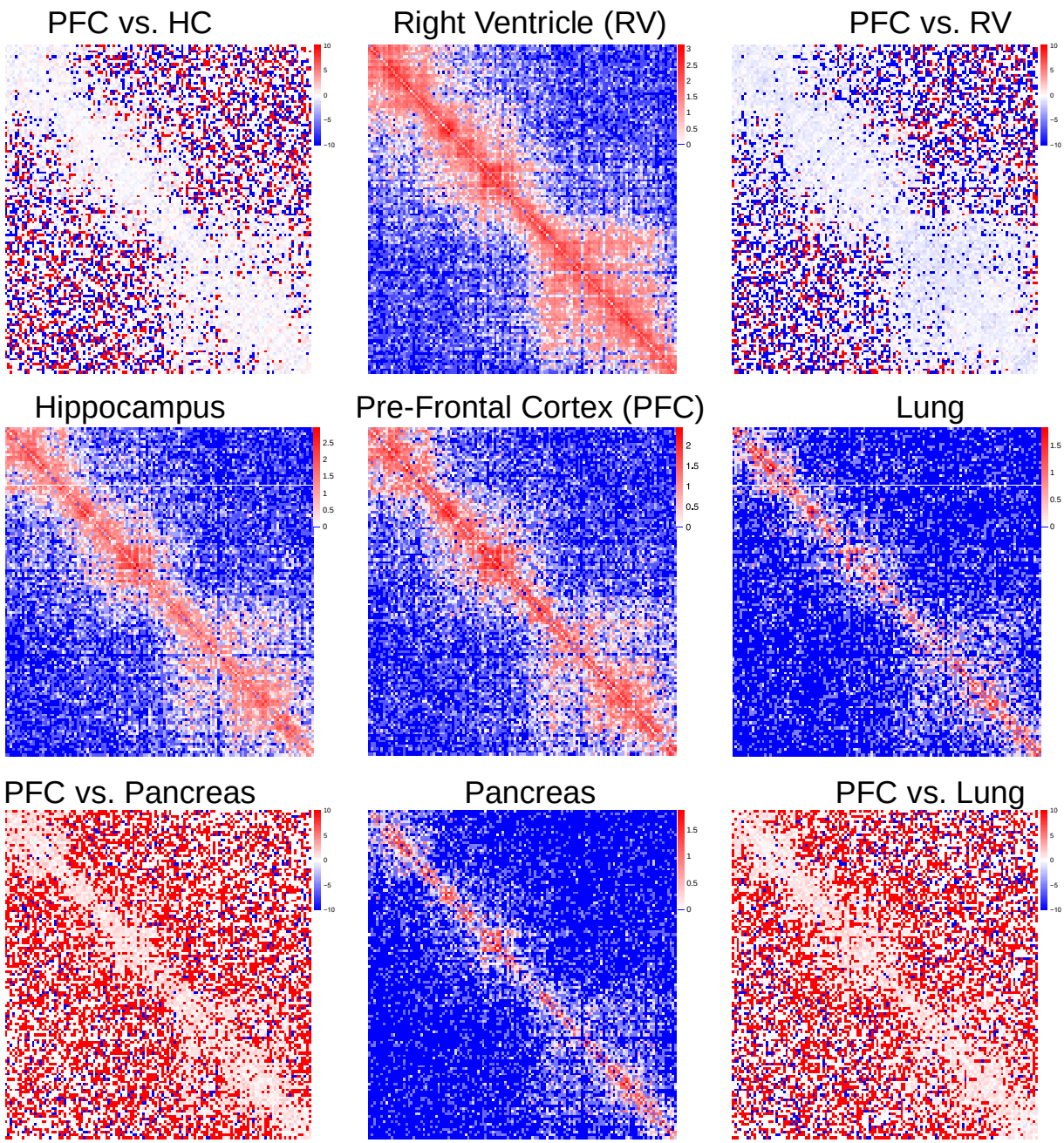

Figure S1 – Tissue and brain regional differences in chromatin conformation. Hi-C contact map heatmaps at 40-kb resolution for a 5-Mb region around *SCN1A* gene. In the central rows and columns are the absolute contact maps, while the corner plots represent the differential contact maps between pre-frontal cortex (PFC) and the indicated tissue. For the latter, red color indicates stronger contacts in PFC in relation to the other tissue, and blue color the opposite.

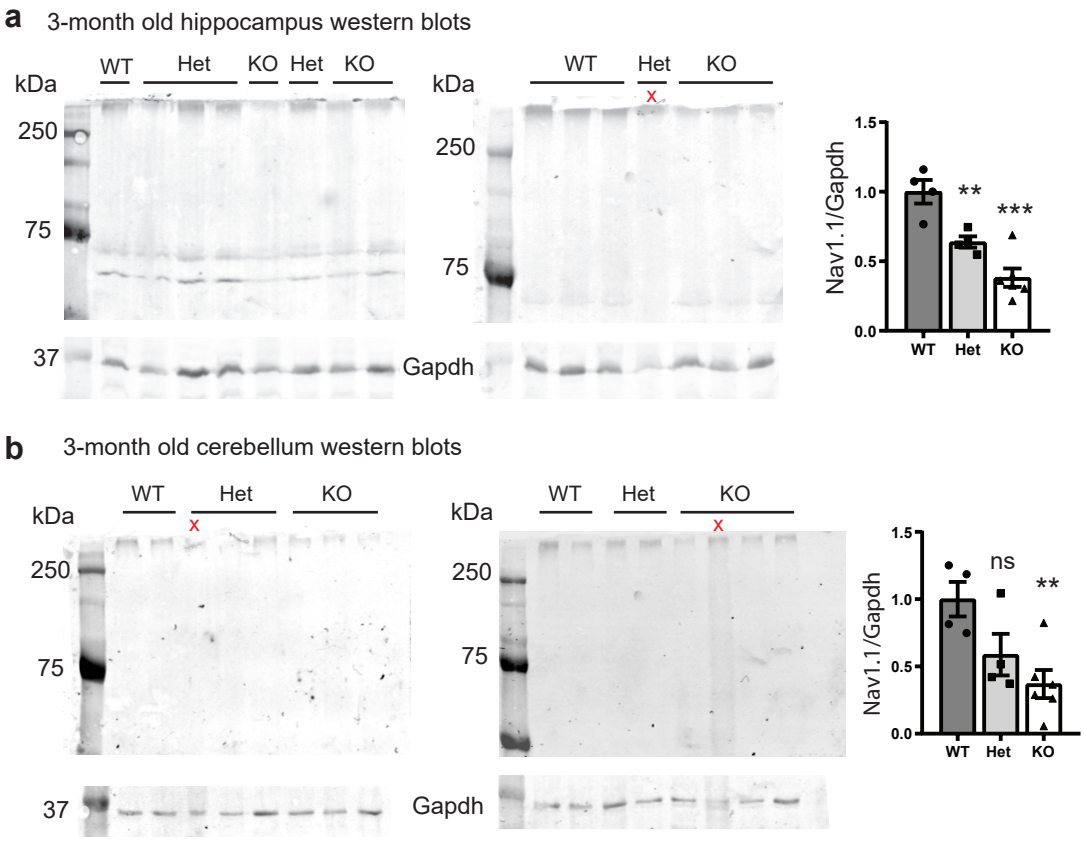

Figure S2: Western blots of NaV1.1 and Gapdh protein in 3-month-old brain lysates. (a) Raw western blots for hippocampus show decrease in NaV1.1 protein abundance in Het (**P = 0.016) and KO (***P = 0.001) mice. (b) Raw western blots for cerebellum show decrease in NaV1.1 protein abundance in Het (P = 0.087) and KO (**P=0.007) mice. WT n = 4, Het n = 4, KO n = 6. Unpaired t-tests used. Error bars represent mean ± sem. Lanes with red cross were not used.

a

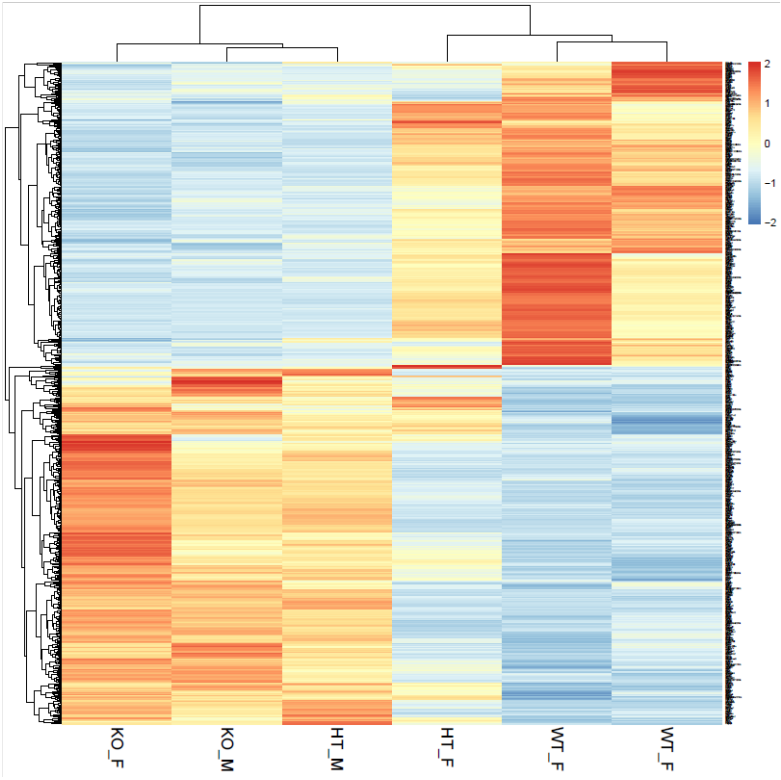

b

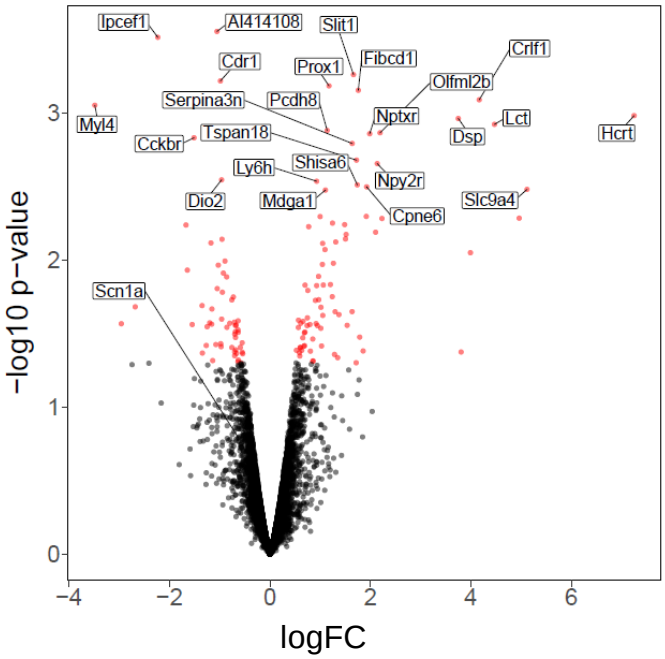

Figure S3: Differential gene expression with *Scn1a 1b* deletion in P32 hippocampus. (a) Heat map of differentially expressed genes. (b) Scatterplot of differentially-expressed genes in Het versus WT mice. Genes with p-value < 0.05 are in red.